Manganese tricarbonyl complexes with asymmetric 2 2-iminopyridine ligands: toward decoupling steric and electronic 3 factors in electrocatalytic CO2 reduction

Article

Accepted Version

Spall, S. J. P., Keane, T., Tory, J., Cocker, D. C., Adams, H., Fowler, H., Meijer, A. J. H. M., Hartl, F. ORCID: https://orcid.org/0000-0002-7013-5360 and Weinstein, J. A. (2016) Manganese tricarbonyl complexes with asymmetric 2 2-iminopyridine ligands: toward decoupling steric and electronic 3 factors in electrocatalytic CO2 reduction. Inorganic Chemistry, 55 (24). pp. 12568-12582. ISSN 0020-1669 doi: 10.1021/acs.inorgchem.6b01477 Available at https://centaur.reading.ac.uk/68114/

www.reading.ac.uk/centaur

CentAUR

Central Archive at the University of Reading

Reading's research outputs online

Inorganic Chemistry

Manganese Tricarbonyl Complexes with Asymmetric 2-Iminopyridine Ligands: Toward Decoupling Steric and Electronic Factors in Electrocatalytic CO2 Reduction

Steven J. P. Spall,[†] Theo Keane,[†] Joanne Tory,[‡] Dean C. Cocker,[†] Harry Adams,[†] Hannah Fowler,[†] Anthony J. H. M. Meijer,[†][iD] František Hartl,*[,‡] and Julia A. Weinstein*[,†][iD]

[†]Department of Chemistry, University of Sheffield, Sheffield S3 7HF, U.K.

[‡]Department of Chemistry, University of Reading, Whiteknights, Reading RG6 6AD, U.K.

Ⓢ Supporting Information

ABSTRACT: Manganese tricarbonyl bromide complexes incorporating IP (2-(phenylimino)pyridine) derivatives, $[MnBr(CO)_3(IP)]$, are demonstrated as a new group of catalysts for CO_2 reduction, which represent the first example of utilization of (phenylimino)pyridine ligands on manganese centers for this purpose. The key feature is the asymmetric structure of the redox-noninnocent ligand that permits independent tuning of its steric and electronic properties. The α-diimine ligands and five new Mn(I) compounds have been synthesized, isolated in high yields, and fully characterized, including X-ray crystallography. Their electrochemical and electrocatalytic behavior was investigated using cyclic voltammetry and UV−vis−IR spectroelectrochemistry within an OTTLE cell. Mechanistic investigations under an inert atmosphere have revealed differences in the nature of the reduction products as a function of steric bulk of the ligand. The direct ECE (electrochemical−chemical−electrochemical) formation of a five-coordinate anion $[Mn(CO)_3(IP)]^-$, a product of two-electron reduction of the parent complex, is observed in the case of the bulky DIPIMP (2-[(((2,6-diisopropylphenyl)imino)methyl]pyridine), TBIMP (2-[(((2-tert-butylphenyl)imino)methyl]-pyridine), and TBIEP (2-[(((2-tert-butylphenyl)imino)ethyl]pyridine) derivatives. This process is replaced for the least sterically demanding IP ligand in $[MnBr(CO)_3(IMP)]$ (2-[(phenylimino)methyl]pyridine) by the stepwise formation of such a monoanion via an ECEC(E) mechanism involving also the intermediate Mn−Mn dimer $[Mn(CO)_3(IMP)]_2$. The complex $[MnBr(CO)_3(IPIMP)]$ (2-[(((2-diisopropylphenyl)imino)methyl]pyridine), which carries a moderately electron donating, moderately bulky IP ligand, shows an intermediate behavior where both the five-coordinate anion and its dimeric precursor are jointly detected on the time scale of the spectroelectrochemical experiments. Under an atmosphere of CO_2 the studied complexes, except for the DIPIMP derivative, rapidly coordinate CO_2, forming stable bicarbonate intermediates, with no dimer being observed. Such behavior indicates that the CO_2 binding is outcompeting another pathway: viz., the dimerization reaction between the five-coordinate anion and the neutral parent complex. The bicarbonate intermediate species undergo reduction at more negative potentials (ca. −2.2 V vs Fc/Fc+), recovering $[Mn(CO)_3(IP)]^-$ and triggering the catalytic production of CO.
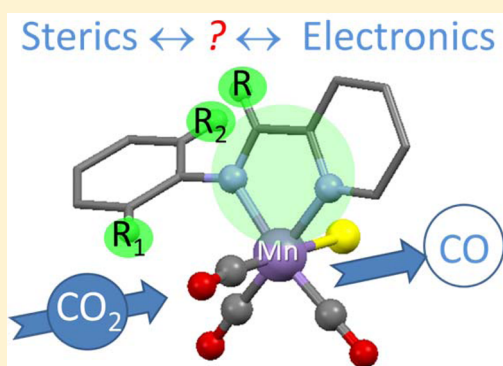
The interest in solar fuels in terms of both photocatalytic and electrocatalytic CO_2 reduction,[1] in the latter case utilizing sustainable electricity, has been increasing markedly in the new millennium. The recent demonstration of the electrocatalytic activity of manganese[2] analogues of the archetypal Re(I) catalysts[3−6] for CO_2 reduction has given a new impetus to research into noble-metal-free catalytic systems. $[MnBr(CO)_3(\alpha\text{-diimine})]$ complexes have been shown to outperform rhenium-based analogues with regard to CO_2 reduction under certain conditions.[7] Most notably, the presence of a Brønsted acid[7−10] appears to be a prerequisite for catalysis with a range of tricarbonyl Mn α-diimine complexes.

Mechanistic studies[5,10] of the active 2,2′-bipyridine-based (R-bpy) manganese catalysts have shown that one-electron reduction of the parent complex $[MnBr(CO)_3(R\text{-bpy})]$ precursor results in the formation of the Mn−Mn dimer $[Mn(CO)_3(R\text{-bpy})]_2$.[8,9] Notably, neither the primary reduction product $[MnBr(CO)_3(R\text{-bpy}^{•-})]$ nor the five-coordinate radical intermediates $[Mn(CO)_3(R\text{-bpy})]^{•}$ have been detected by either UV−vis or IR spectroscopy.[2,7] Nanosecond time-resolved infrared (TRIR) studies reveal that no detectable solvent adduct is formed before the dimerization of Mn species on this time scale; instead, the five-coordinate species is observed, which rapidly dimerizes.[10] For some of the Re analogues, a one-electron-reduced complex, $[ReCl(CO)_3(R\text{-bpy}^{•-})]$, was observed by IR spectroscopy and identified by the ca. 15−20 cm^{-1} decrease in the $\tilde{\nu}(CO)$ energy,[11−13] as was the

62 five-coordinate radical $[Re(CO)_3(^tBu\text{-}bpy)]^\bullet$ by an additional
63 15−20 cm^{-1} shift.

64   Two mechanisms have been proposed[10,14−18] for the
65 ultimate reduction of $[Mn(CO)_3(\alpha\text{-diimine})]_2$ in the presence
66 of CO_2, which can be referred to as the anionic and the
67 oxidative addition[19] pathways. The anionic pathway involves
68 reduction of the dimer $[Mn(CO)_3(\alpha\text{-diimine})]_2$ at a potential
69 more negative than that of the parent complex, generating the
70 five-coordinate anion $[Mn(CO)_3(\alpha\text{-diimine})]^-$, to which CO_2
71 coordinates and is catalytically reduced in the presence of a
72 Brønsted acid (the source of H$^+$). The anionic pathway is
73 broadly similar to the two-electron pathway observed for Re
74 complexes.[20,21] In contrast, the uncommon second pathway
75 identified using pulsed EPR studies[19] involves coordination of
76 CO_2 to the dimer $[Mn(CO)_3(2,2'\text{-bpy})]_2$ in the presence of a
77 Brønsted acid in a concerted oxidative addition step. This
78 process is shown to generate a low-spin Mn^{II}−COOH complex,
79 from which CO is subsequently released.

80   Since the catalytic CO_2 reduction with the use of
81 $[MnX(CO)_3(\alpha\text{-diimine})]$ (α-diimine = R-bpy; X = halide or
82 pseudohalide) has been shown to proceed in many cases via a
83 dimerization step, immobilization of the catalyst[22] or
84 introduction of sterically hindering groups at bpy may have a
85 profound effect on the catalytic activity.[23] Indeed, it has
86 recently been shown that the use of bipyridines incorporating
87 bulky groups in the 6,6'-positions[24,25] (or another bulkier
88 heterocyclic ligand[26]) largely inhibits dimerization in the
89 catalytic cycle. The result is the formation of the stable five-
90 coordinate anion via the two-electron transfer (ECE) at the first
91 cathodic wave. However, coordination of CO_2 to the five-
92 coordinate anion produces a stable species which must be
93 reduced at considerably more negative potentials[27] in order for
94 catalysis to be observed. It has recently been shown that in the
95 presence of a Lewis acid, Mg^{2+},[7,28] the catalytic overpotential[29]
96 is decreased by approximately 400 mV.

97   A similar behavior was observed for $[MnBr(CO)_3(R\text{-DAB})]$
98 complexes featuring nonaromatic 1,4-diazabuta-1,3-diene (R-
99 DAB)[8,9,30] ligands. The reduction potentials of the dimers
100 $[Mn(CO)_3(R\text{-DAB})]_2$ are almost identical with those of the
101 parent complexes, implying that the five-coordinate anion is
102 produced directly upon reduction and reacts readily with CO_2
103 in solution to form a stable bicarbonate complex[8,30] and, as
104 with sterically hindered 2,2'-bipyridine ligands,[25] a much more
105 negative potential (below 2 V vs Fc/Fc$^+$) must be applied to
106 trigger catalytic CO_2 reduction. Functionalization of the α-
107 diimine with a sterically bulky group such as ^tBu should also
108 modify the electronic properties of the ligand. In particular, this
109 change should affect the energy of the LUMO, the reduction
110 potential, and catalytic activity.[23−33]

111   Introducing steric bulk[23,25] to prevent unwanted reactions of
112 the catalytic species, including dimerization as either Mn−Mn[9]
113 or C(imino)−C(imino) bound species,[21] while at the same
114 time reducing the risk of increased overpotential is a
115 challenging task. Molecular designs that allow for steric and
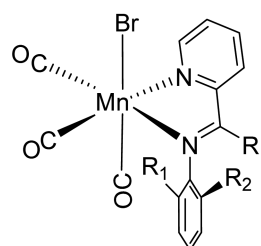116 electronic effects to be decoupled are required.

117   In this paper we have investigated a family of tricarbonyl
118 manganese complexes featuring asymmetric α-diimine ligands,
119 iminopyridines (IP).[21,23,34,35] They combine an accessible
120 −C═N− imino bond of the diazabuta-1,3-diene derivatives
121 DAB[32] with the aromatic pyridine part, thereby being a
122 "hybrid" of 2,2'-bipyridine ligands and nonaromatic R-DAB
123 ligands. Each of the parts is important: for instance, a Mn(I)
124 complex with Ph-DAB demonstrates formation of five-

125 coordinate anions, with the steric bulk of the ligand preventing
126 dimerization, but does not act as a catalyst for CO_2 reduction
127 due to insufficiently negative reduction potential.[8]

128   Introduction of the pyridine moiety allows one to reach the
129 required reduction potentials, while the Ph group attached to
130 the C═N fragment can be decorated with sterically demanding
131 substituents, ensuring steric bulk while only slightly affecting
132 the electronic properties. As the phenyl moiety lies out of plane
133 with the conjugated α-diimine (because of steric effects), the π
134 electrons of the phenyl substituent are decoupled from the
135 metallacycle formed by the metal center and the α-diimine.
136 Therefore, functionalization of the phenyl ring in the R$_1$ and R$_2$
137 positions with large sterically hindering groups (that also have a
138 +I effect) will have only very minimal effects on the electronics
139 of the active site of the molecule (vide infra). These ligands
140 offer an opportunity to separate steric and electronic effects in a
141 chelating α-diimine ligand to a certain extent. Thus, the
142 possibility arises of a systematic variation of the steric hindrance
143 by changing R$_1$ and R$_2$ groups, while the R group strongly
144 influences the electronics (but could also hinder the C═N
145 bond).

146   These ligands are readily accessible via simple synthetic
147 routes, which are suitable for the purpose of comparatively
148 independent alteration of steric and electronic effects (Chart 1).

Chart 1. General Structure of the Complexes with the Asymmetric α-Diimine Ligands (2-R$_1$-6-R$_2$-phenyl)(R-imino)pyridine[a]

Ligand	R	R$_1$	R$_2$
IMP (1)	H	H	H
IPIMP (2)	H	^iPr	H
DIPIMP (3)	H	^iPr	^iPr
TBIMP (4)	H	^tBu	H
TBIEP (5)	CH$_3$	^tBu	H

[a]Numbers given in parentheses correspond to the Mn complexes. When R = H, the ligands will be derivatives of [(phenylimino)-methyl]pyridine: IMP (R$_{1,2}$ = H), IPIMP (R$_1$ = ^iPr, R$_2$ = H), and DIPIMP (R$_{1,2}$ = ^iPr), TBIMP (R$_1$ = ^tBu, R$_2$ = H). R = CH$_3$ gives TBIEP, [(($tert$-butylphenyl)imino)ethyl]pyridine.

149   The potential of such ligands[34−38] has been convincingly
150 illustrated by the recent work on a Re tricarbonyl complex with
151 2-[((2-cyclohexyl-1-methyl)methyl)imino]pyridine[36] (both the
152 one-electron-reduced parent complex and the neutral five-
153 coordinate Re(0) species were detected), and Mo pyridine-
154 monoimides.[34]

155   Herein we report a new series of manganese-based catalysts
156 for CO_2 reduction. We will show that a change in the structure
157 of the ligands within the same series affects the efficiency of the
158 process and the relative distribution of the intermediate species,
159 demonstrating the versatile and tunable nature of these types of
160 catalysts.

■ EXPERIMENTAL SECTION

162 All solvents were supplied by VWR and used as received. The
163 compounds were purchased from either Sigma-Aldrich or Strem
164 Chemicals and, unless stated, used as received. Tetrabutylammonium
165 hexafluorophosphate, [Bu$_4$N][PF$_6$], was recrystallized from hot
166 ethanol and dried overnight in a vacuum oven before use in the
167 electrochemical studies. TBIEP (2-[((2-$tert$-butylphenyl)imino)ethyl]-

pyridine) and TBIMP were synthesized as previously described;[35] the analytical data matched those reported previously. Unless otherwise stated, UV−vis spectra were recorded on a Carry 50 Bio spectrophotometer and IR spectra on a PerkinElmer Spectrum 1 FT-IR spectrometer.

Syntheses. *IMP (2-[(Phenylimino)methyl]pyridine).* Aniline (11.3 mmol, 1.05 g, 1.02 mL) was added to 2-pyridinecarboxaldehyde (11.3 mmol, 1.2 g, 1.1 mL) in flame-dried glassware and stirred for 1 h. Hexane (10 mL) was added and the solution dried over sodium sulfate. The solution was filtered, concentrated under vacuum, and placed in a freezer overnight. The large yellow needlelike crystals that formed were filtered and washed with hexane. Yield: 73%. ^{1}H NMR (400 MHz, CDCl$_3$): δ 8.72 (d, J = 4.7 Hz, 1H), 8.61 (s, 1H), 8.21 (d, J = 7.9 Hz, 1H), 7.83 (td, J = 7.7, 1.6 Hz, 1H), 7.47−7.35 (m, 3H), 7.29 (d, J = 7.7 Hz, 3H), 1.58 (s, 4H).

IPIMP (2-[2-((Isopropylphenyl)imino)methyl]pyridine). 2-Isopropylaniline (12.4 mmol, 1.7 g, 1.8 mL) was mixed with 2-pyridinecarboxaldehyde (12.4 mmol, 1.3 g, 1.2 mL) in flame-dried glassware and stirred for 1 h. Hexane (20 mL) was added and the solution dried over sodium sulfate. The solution was filtered and solvent removed under vacuum, yielding the product as a brown oil. Previous reports indicated that this compound could not be crystallized; therefore, the oil was used in the next reaction step without further purification (purity by NMR >97%). ^{1}H NMR (400 MHz, CDCl$_3$): δ 8.72 (ddd, J = 4.8, 1.6, 0.9 Hz, 1H), 8.54 (s, 1H), 8.26 (dd, J = 7.9, 0.9 Hz, 1H), 7.82 (ddd, J = 7.9, 1.7, 0.8 Hz, 1H), 7.45−7.32 (m, 2H), 7.31−7.22 (m, 2H), 7.08−6.96 (m, 1H), 3.56 (dp, J = 13.8, 6.8 Hz, 1H), 1.26 (dd, J = 6.8, 4.1 Hz, 7H).

DIPIMP (2-[((2,6-Diisopropylphenyl)imino)methyl]pyridine). 2,6-Diisopropylaniline (11.3 mmol, 2 g, 2.1 mL) was mixed with 2-pyridinecarboxaldehyde (11.3 mmol, 1.2 g, 1.1 mL) in flame-dried glassware and stirred for 2 h. Hexane (10 mL) was added and the solution dried over sodium sulfate. The solution was filtered and concentrated before being placed in a freezer overnight. Light brown to yellow crystals were formed, which were filtered off and washed with hexane. Yield: 67%. ^{1}H NMR (400 MHz, CDCl$_3$): δ 8.73 (ddd, J = 4.8, 1.7, 0.9 Hz, 1H), 8.31 (s, 1H), 8.27 (dt, J = 7.9, 1.0 Hz, 1H), 7.90−7.82 (m, 1H), 7.42 (ddd, J = 7.5, 4.9, 1.2 Hz, 1H), 7.22−7.07 (m, 3H), 2.97 (hept, J = 6.9 Hz, 2H), 1.62 (s, 1H), 1.18 (d, J = 6.9 Hz, 13H).

Complexes **1**−**6** were prepared from [MnBr(CO)$_5$] and the corresponding ligand, using diethyl ether as a solvent. The products were collected by centrifugation and washed with diethyl ether to afford analytically pure **1**−**6**. ^{1}H NMR spectra for **1**−**5** are given in Figure SI22−SI26 in the Supporting Information.

[MnBr(CO)$_3$(IMP)] (1). [MnBr(CO)$_5$] (1.1 mmol, 0.3 g) was combined with IMP (1.1 mmol, 0.2 g) in diethyl ether (20 mL) and refluxed under aerobic conditions for 4 h.[39] The product was formed in quantitative yield. ^{1}H NMR (500 MHz, CDCl$_3$): δ 9.26 (d, J = 5.0 Hz, 1H), 8.45 (s, J = 27.9 Hz, 1H), 8.14−7.79 (m, 3H), 7.68−7.36 (m, 5H). HRMS (TOF-ES, + ve): m/z (M + Na$^+$) calcd for C$_{15}$H$_{10}$N$_2$O$_3$NaBrMn 422.9153, found 422.9149.

[MnBr(CO)$_3$(IPIMP)] (2). [MnBr(CO)$_5$] (0.89 mmol, 0.24 g) was combined with IPIMP (0.89 mmol, 0.2 g) in diethyl ether (20 mL) and refluxed under aerobic conditions for 4 h. The product was formed in quantitative yield. ^{1}H NMR (500 MHz, CDCl$_3$): δ 9.27 (s, 1H), 8.39 (s, 1H), 8.04 (s, 1H), 7.94 (d, J = 4.1 Hz, 1H), 7.78 (d, J = 7.0 Hz, 1H), 7.61 (s, 1H), 7.48 (d, J = 15.3 Hz, 1H), 7.43 (d, J = 6.7 Hz, 1H), 7.37 (t, 1H), 7.30 (d, J = 6.9 Hz, 1H), 3.58 (s, 1H), 3.03 (d, J = 35.6 Hz, 1H), 1.47−1.11 (m, 1H). HRMS (TOF-ES, +ve): m/z (M + Na$^+$) calcd for C$_{18}$H$_{16}$N$_2$O$_3$NaBrMn 464.9622, found 464.9644.

[MnBr(CO)$_3$(DIPIMP)] (3). [MnBr(CO)$_5$] (0.75 mmol, 0.2 g) was combined with DIPIMP (0.75 mmol, 0.2 g) in diethyl ether (20 mL) and refluxed under aerobic conditions for 4 h. The product was formed in 97% yield. ^{1}H NMR (500 MHz, CDCl$_3$): δ 9.30 (s, 1H), 8.41 (s, 1H), 7.99 (d, J = 50.7 Hz, 2H), 7.63 (s, 1H), 7.34 (s, 2H), 4.04 (s, 1H), 2.91 (s, 1H), 1.34 (d, J = 3.1 Hz, 6H), 1.05 (dd, J = 80.6, 35.1 Hz, 6H). HRMS (TOF-ES, +ve): m/z (M + Na$^+$) calcd for C$_{21}$H$_{22}$N$_2$O$_3$NaBrMn 507.0092, found 507.0107.

[MnBr(CO)$_3$(TBIMP)] (4). [MnBr(CO)$_5$] (0.84 mmol, 0.23 g) was combined with DIPIMP (0.84 mmol, 0.2 g) in diethyl ether (20 mL) and refluxed under aerobic conditions for 4 h. The product was formed in quantitative yield. ^{1}H NMR (400 MHz, CDCl$_3$): δ 9.27 (d, J = 4.4 Hz, 1H), 8.50 (s, 1H), 8.12 (d, J = 6.9 Hz, 1H), 8.03 (t, J = 7.2 Hz, 1H), 7.91 (d, J = 7.1 Hz, 1H), 7.61 (t, J = 6.2 Hz, 1H), 7.57 (d, J = 7.4 Hz, 1H), 7.30 (t, 1H), 1.43 (s, 1H). HRMS (TOF-ESI, +ve): m/z (M + Na$^+$) calcd for C$_{19}$H$_{18}$N$_2$O$_3$NaBrMn 478.9774, found 478.9789.

[MnBr(CO)$_3$(TBIEP)] (5). [MnBr(CO)$_5$] (0.8 mmol, 0.22 g) was combined with TBIEP (0.8 mmol, 0.2 g) and refluxed under aerobic conditions in diethyl ether (20 mL) for 4 h. The product was formed in quantitative yield. ^{1}H NMR (400 MHz, CDCl$_3$): δ 9.28 (d, J = 5.0 Hz, 1H), 8.04 (td, J = 7.8, 1.3 Hz, 1H), 7.95 (d, J = 7.7 Hz, 1H), 7.88 (dd, J = 6.1, 3.4 Hz, 1H), 7.65−7.54 (m, 2H), 7.34−7.27 (m, 2H), 2.39 (s, 3H), 1.39 (s, 8H). HRMS (TOF-ES, +ve): m/z (M + Na$^+$) calcd for C$_{20}$H$_{20}$N$_2$O$_3$NaBrMn 492.9935, found 492.9934.

[MnBr(CO)$_3$(bpy)] (6). This compound was prepared following the literature procedure;[2] analytical data are in agreement with the literature data. [MnBr(CO)$_5$] (1.28 mmol, 0.35 g) was combined with 2,2'-bipyridine (1.28 mmol, 0.2 g) in diethyl ether (20 mL) and refluxed under aerobic conditions for 4 h. The product was formed in 80% yield. ^{1}H NMR (500 MHz, CDCl$_3$): δ 9.27 (d, J = 4.3 Hz, 1H), 8.12 (d, J = 6.5 Hz, 1H), 7.99 (t, 1H), 7.53 (t, 1H). HRMS (TOF-ESI, +ve): m/z (M + Na$^+$) calcd for C$_{13}$H$_8$N$_2$O$_3$NaBrMn 396.8991, found 369.8988.

Cyclic Voltammetry. Cyclic voltammetry was performed using a Princeton Applied Research VersaSTAT3 potentiostat on 2 mM **1**−**6** in Grubbs dried HPLC-grade acetonitrile containing 2×10^{-1} M [Bu$_4$N][PF$_6$] as supporting electrolyte. A glassy-carbon working electrode (surface area 0.07 cm^2, polished on alumina and paper) and a Pt-wire counter electrode were used with a 0.1 M KCl Ag/AgCl reference electrode.

The solutions were deoxygenated by bubbling thoroughly with bottled N$_2$ (BOC), and the N$_2$ atmosphere was maintained over the samples during the experiment. To test for catalytic current in the presence of CO$_2$, the samples were bubbled thoroughly with bottled CO$_2$ (BOC) and cyclic voltammograms (CVs) were recorded under an atmosphere of CO$_2$ (some residual water might be present in the CO$_2$ used to saturate the samples). Water was then added (0.3−6 mL of the solution of each sample) to test the effects of Brønsted acid. Ferrocene was added as the internal standard at the end of all experiments.

Spectroelectrochemistry. Infrared spectroelectrochemistry was performed using an EmStat3 or EmStat3+ potentiostat (PalmSens, Houten, The Netherlands). The solution of 4 mM complex in the presence of 3×10^{-1} M [Bu$_4$N][PF$_6$] in dry acetonitrile was analyzed using an optically transparent thin-layer electrochemical (OTTLE) cell equipped with Pt minigrid working and auxiliary electrodes, an Ag-microwire pseudoreference electrode, and CaF$_2$ windows. Samples were prepared under an argon atmosphere; for electrocatalytic measurements, the solutions were bubbled with CO$_2$ on a frit (a few minutes) to saturation under normal pressure. Parallel IR and UV−vis spectral monitoring during the spectroelectrochemical experiment was performed on a Bruker Vertex 70v FT-IR spectrometer or PerkinElmer Spectrum 1 and a Scinco S-3100 spectrophotometer, respectively. Thin-layer CVs were recorded in the course of the experiment.

Gas Chromatography Linked to Electrolysis. Bulk electrolysis was performed on a 0.17 mM solution of each of the complexes in a 60 mL solution of acetonitrile/water (9/1 v/v). The cell setup consisted of a Pt-mesh working electrode, a Pt-rod counter electrode in a semiporous compartment, and an Ag-wire pseudoreference electrode in a 0.1 M KCl solution. The potential of the Fc/Fc$^+$ recorded in this setup using a glassy-carbon 3 mm diameter electrode was +0.350 V vs Ag wire pseudoreference. Hence, in order to reach the potential necessary for the CO$_2$ reduction as estimated from the CV data, the potential was held at −1.9 V vs Ag wire for all samples: i.e., −2.25 V vs Fc/Fc$^+$. Prior to electrolysis, a CV was recorded in the bulk electrolysis cell using a glassy-carbon working electrode. Gas samples (100 μL) were withdrawn from the head space at regular intervals and analyzed

307 by a gas chromatograph fitted with a thermal conductivity detector
308 (Perkin ElmerArnel autosystem XL). H$_2$ was used as the carrier gas in
309 CO-quantification experiments. N$_2$ was used as a carrier gas in the
310 control experiment.

311 **X-ray Crystallography.** Crystals were grown using the antisolvent
312 crystallization method, with the solvent dichloromethane and hexane
313 as the antisolvent. Single-crystal X-ray diffraction data were collected
314 on a Bruker SMART APEX-II CCD diffractometer operating a Mo Kα
315 sealed-tube X-ray source or a Bruker D8 Venture diffractometer
316 equipped with a PHOTON 100 dual-CMOS chip detector and
317 operating a Cu Kα IμS microfocus X-ray source. The data were
318 processed using Bruker APEX3 software and corrected for absorption
319 using empirical methods (SADABS) based upon symmetry-equivalent
320 reflections combined with measurements at different azimuthal
321 angles.[40] The crystal structures were solved and refined using the
322 Bruker SHELXTL software package.

323 **Computational Methods.** Density functional theory (DFT)
324 calculations were performed using the Gaussian 09 program package.[41]
325 All calculations utilized the global hybrid exchange correlation
326 functional B3LYP,[42,43] a "mixed" basis set consisting of the SDD
327 basis set as defined in Gaussian for Mn and the 6-311G(d,p) basis set
328 for all other atoms.[44−47] The solvent acetonitrile was included using
329 the polarizable continuum model (PCM) as implemented in
330 Gaussian.[48,49] All species were modeled at the lowest multiplicity
331 appropriate for the electron count, and the restricted formalism was
332 used for closed-shell cases. An "ultrafine" integral grid, as defined by
333 Gaussian, was used and all geometries were confirmed as minima by
334 the absence of imaginary frequencies in their vibrational spectra as
335 calculated within the harmonic approximation. The values of
336 vibrational frequencies have been scaled by 0.966 to match
337 experimental $\nu(CO)$ values of the parent neutral complexes.

■ RESULTS AND DISCUSSION

339 **X-ray Crystallography.** The crystal structures of the
340 complexes [MnBr(CO)$_3$(α-diimine)] (α-diimine = TBIEP,
341 IMP, IPIMP, DIPIMP) are shown in Figure 1, and selected
342 bond distances and angles are given in Table SI1 in the
343 Supporting Information. Similar bond lengths are observed for
344 the four complexes, and these are in good agreement with
345 related [MnBr(CO)$_3$(α-diimine)] species reported in the
346 literature. The X-ray data are in good agreement with the
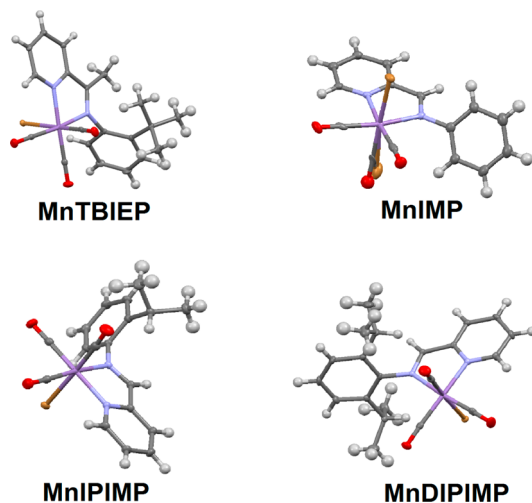347 results obtained through DFT calculations. As predicted by

Figure 1. X-ray crystal structures of the studied complexes shown with
thermal ellipsoids at the 50% probability level. CCDC 1457930
(MnTBIEP), 1457931 (MnDIPIMP), 1457932 (MnIPIMP), 1457933
(MnIMP). Full crystallographic details are given in the Supporting
Information.

348 DFT, the pyridine and phenyl rings lie approximately
349 orthogonally to one another (dihedral angles between the
350 corresponding planes are MnTBIEP 84.55°, MnIPIMP 83.64°,
351 MnDIPIMP 78°), resulting in little orbital overlap between
352 these two moieties, with the exception of MnIMP, where the
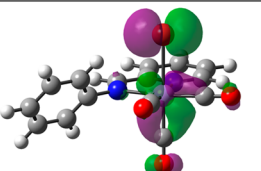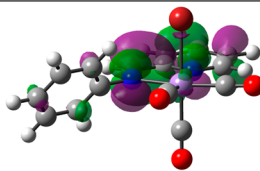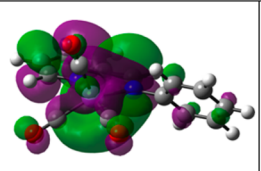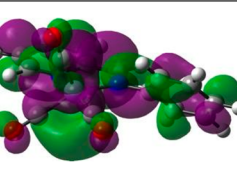353 two ring systems were significantly less orthogonal (56.54°).
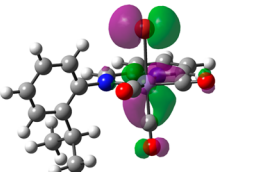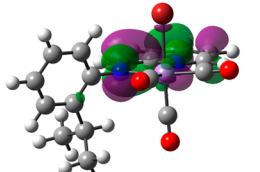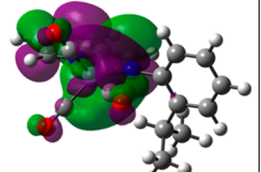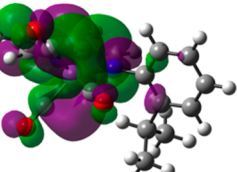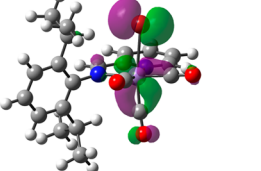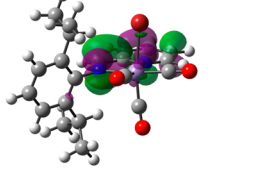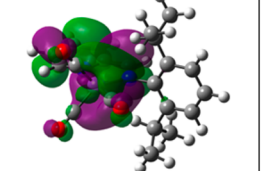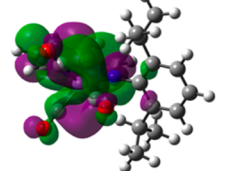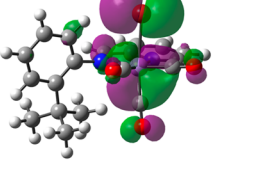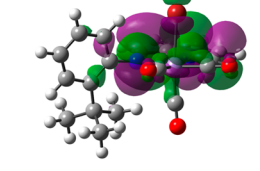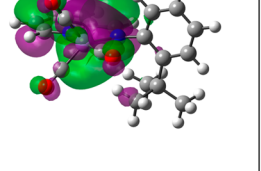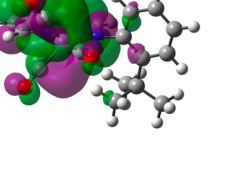
354 The crystal structures have revealed significant steric
355 hindrance between the substituents R = Me and R$_1$ = ^{t}Bu in
356 MnTBIEP, which inhibits rotation of the Ph ring and confers
357 conformational rigidity. Rotation of the Ph ring in MnDIPIMP
358 is also inhibited by the two ^{i}Pr groups and hence also has
359 conformational rigidity. In contrast, MnIMP and MnIPIMP
360 exhibit much smaller steric hindrance, facilitating the rotation of
361 the phenyl ring.

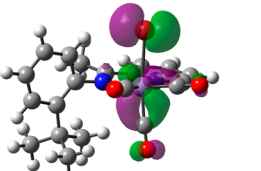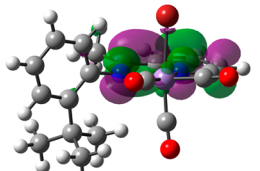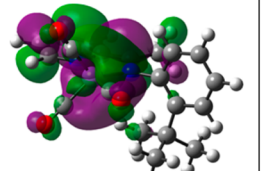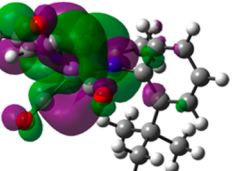362 **Computational Investigations of Molecular Structures**
363 **and Frontier Orbitals by DFT.** The optimized geometries of
364 the studied complexes with frontier orbitals overlaid as
365 calculated by DFT are displayed in Table 1. As anticipated,
366 the phenyl group lies out of the plane of the chelating diimine.
367 The HOMO is localized predominantly over the axial Br−Mn−
368 C(O) bonds with almost no contribution from the phenyl
369 moiety. The LUMO resides largely on the imine, pyridyl, and
370 metal center, with minimal contribution from the C1−C2 and
371 C1−C6 σ bonds of the phenyl groups. In the case of MnIMP,
372 due to the lack of substitution at R$_1$ and R$_2$, the phenyl moiety
373 is less sterically hindered and thus is positioned closer to the
374 plane of the imino-pyridine fragment, resulting in a small
375 degree of involvement of the phenyl π system in the low-energy
376 unoccupied orbitals. This trend continues in the other low-
377 energy unoccupied orbitals (see Figures SI1−SI10 in the
378 Supporting Information).

379 The energies of the HOMO in all complexes are within 0.02
380 eV of each other, and all compounds in the IMP subset of
381 complexes have a LUMO that lies within 0.03 eV of those of
382 the other complexes. In contrast, MnTBIEP shows a difference
383 in LUMO energy of +0.19 eV in comparison with IPIMP. This
384 larger difference in LUMO energy comes as result of
385 methylation at the R position. In contrast, adding two isopropyl
386 groups at the R$_1$ and R$_2$ positions resulted in an energy
387 difference of just 0.02 eV between MnIMP and MnDIPIMP.
388 The results of the calculations on the trends in the energies of
389 HOMO/LUMO are in full agreement with the experimentally
390 determined redox potentials (see below). These results imply
391 that an almost complete separation between the steric and the
392 electronic effects in the context of few-electron reductions can
393 indeed be achieved in this series of complexes. Changing the R
394 group will strongly affect the energy of the LUMO while also
395 having some impact on the steric properties at the carbon of
396 the imino C=N bond, while changing the R$_1$ or R$_2$ groups
397 should have considerable effects on the steric hindrance of the
398 molecule (protecting the Mn and imino-N centers) but hardly
399 affect its electronic properties.

400 The experimental and calculated carbonyl vibrational
401 frequencies of the studied complexes are shown in Table 2.
402 The calculated frequencies are in good agreement with the
403 experimental values. Some systematic discrepancies are
404 apparent: the high-energy A′(1) mode tends to be under-
405 estimated by ∼10 cm^{-1}, the A″ mode tends to have a lower
406 deviation of only ∼2 cm^{-1}, and the low-energy A′(2) mode
407 tends to be overestimated by ∼10 cm^{-1}. It is clear that
408 attachment of the methyl group as R increases the electron
409 density on the metal center and thus also the Mn to CO π
410 back-bonding, as evidenced by the smaller values of $\nu(CO)$ for

Table 1. Frontier Orbitals of the Complexes 1−5 and the Corresponding Five-Coordinate Anions Calculated at the B3LYP/ SDD+6-311G(d,p)/IEFPCM Level[a]

HOMO	LUMO	HOMO	LUMO
Parent Complex		Five-coordinate anion	
MnIMP		MnIMP	

ε = -6.31 eV	ε = -2.84 eV	ε = -3.67 eV	ε = -1.18 eV
MnIPIMP		MnIPIMP	

ε = -6.33 eV	ε = -2.81 eV	ε = -3.70 eV	ε = -1.01 eV
MnDIPIMP		MnDIPIMP	

ε = -6.31 eV	ε = -2.83 eV	ε = -3.67 eV	ε = -0.99 eV
MnTBIMP		MnTBIMP	

ε = -6.36 eV	ε = -2.80 eV	ε = -3.64 eV	ε = -1.02 eV
MnTBIEP		MnTBIEP	

[a]Isovalue of 0.04 (e bohr^{-3})$^{1/2}$.

MnTBIEP in comparison to the IMP subseries (complexes 1− 4). However, substitution at R_1 and R_2 has only a slight effect on the frequencies. It should be noted that the magnitude of these effects is small (<10 cm^{-1}) and that it is beyond the scope of this computational work to unravel the various factors effecting changes in CO stretching frequencies.[50]

The results of DFT calculations (Table 2) of IR spectra for the parent Br complexes [MnBr(CO)$_3$(αdiimine)] (1−5) and the corresponding [Mn(CO)$_3$(H$_2$O)(α-diimine)]$^+$ (cationic aquo complexes) match the experimental data well. We therefore use the calculated ν(CO) wavenumbers for the hydrolyzed aquo and reduced (dimer and anion) species to aid the analysis of the IR spectra and product assignment in the course of the corresponding cathodic IR-SEC experiments (vide infra).

Adding electron-donating groups (^{i}Pr, ^{t}Bu) to the phenyl ring of the IMP subseries does not have a large effect on the ν(CO) frequency, the band positions being virtually unchanged

Table 2. Experimentally Obtained and Calculated Frequencies of Carbonyl Stretching Vibrations, ν(CO), of the Mn Complexes in Their Neutral Form (1−5) and Transient One-Electron-Reduced Form, as well as Five-Coordinate Anion, a Cationic Aqua Complex, and an Mn−Mn Bound Dimer[a]

	ν(CO)/cm^{-1}	
species	calcd	exptl
[MnBr(CO)$_3$(IMP)] (**1**)	2020, 1943, 1931	2029, 1941, 1926
[MnBr(CO)$_3$(IMP)]$^-$	1992, 1906, 1897	not obsd
[Mn(CO)$_3$(H$_2$O)(IMP)]$^+$	2046, 1966, 1957	2051, 1964, 1958[b]
[Mn(CO)$_3$(IMP)]$^-$	1906, 1830, 1813	1930, 1826
[Mn(CO)$_3$(IMP)]$_2$	1964, 1918, 1891, 1882, 1872, 1868	1994, 1949, 1902, 1875
[MnBr(CO)$_3$(IPIMP)] (**2**)	2020, 1945, 1929	2029, 1943, 1923
[MnBr(CO)$_3$(IPIMP)]$^-$	1988, 1905, 1891	not obsd
[Mn(CO)$_3$(H$_2$O)(IPIMP)]$^+$	2044, 1963, 1956	2049, 1959 (br)
[Mn(CO)$_3$(IPIMP)]$^-$	1905, 1826, 1808	1929, 1824
[Mn(CO)$_3$(IPIMP)]$_2$	1964, 1917, 1890, 1881, 1866, 1860	1981, 1949, 1901, 1882, 1862
[MnBr(CO)$_3$(DIPIMP)] (**3**)	2019, 1945, 1929	2028, 1944, 1922
[MnBr(CO)$_3$(DIPIMP)]$^-$	1985, 1906, 1890	not obsd
[Mn(CO)$_3$(H$_2$O)(DIPIMP)]$^+$	2045, 1964, 1957	2050, 1960 (br)[b]
[Mn(CO)$_3$(DIPIMP)]$^-$	1903, 1824, 1806	1929, 1829/1822
[Mn(CO)$_3$(DIPIMP)]$_2$	1965, 1918, 1890, 1880, 1860, 1850	not obsd
[MnBr(CO)$_3$(TBIMP)] (**4**)	2020, 1947, 1925	2029, 1945, 1923
[MnBr(CO)$_3$(TBIMP)]$^-$	1988, 1907, 1890	not obsd
[Mn(CO)$_3$(H$_2$O)(TBIMP)]$^+$	2045, 1965, 1956	not obsd
[Mn(CO)$_3$(TBIMP)]$^-$	1906, 1827, 1807	1928, 1823
[Mn(CO)$_3$(TBIMP)]$_2$	1964, 1916, 1889, 1879, 1862, 1854	not obsd
[MnBr(CO)$_3$(TBIEP)] (**5**)	2018, 1944, 1921	2028, 1943, 1917
[MnBr(CO)$_3$(TBIEP)]$^-$	1980. 1904, 1883	not obsd
[Mn(CO)$_3$(H$_2$O)(TBIEP)]$^+$	2042, 1962, 1950	2048, 1960, 1954
[Mn(CO)$_3$(TBIEP)]$^-$	1897, 1819, 1798	1922, 1814 (br)
[Mn(CO)$_3$(TBIEP)]$_2$	1958, 1909, 1880, 1870, 1850, 1841	not obsd

[a]In acetonitrile at 293 K. [b]Positions are approximate, as the parent CO stretching vibrations obscure those of the cationic aqua complex.

among complexes **1−4**. The two higher-frequency bands are at 2028−2029 and 1943−1944 cm^{-1} for all five complexes, while the lowest ν(CO) band is seen at 1923−1922 cm^{-1} for the IMP series but is shifted to lower energy, 1917 cm^{-1} in [MnBr(CO)$_3$(TBIEP)], where the increased π back-donation is caused by R = Me. This invariability of ν(CO) frequencies, while the dihedral angles between the planes of the pyridine and phenyl moieties of the IP ligands are clearly changing drastically, from ∼56 to ∼84°, confirms the opportunity of the somewhat independent tuning of electronic and steric factors.

Calculations performed on the five-coordinate anions of the studied compounds, [Mn(CO)$_3$(diimine)]$^-$, show trends very similar to what has been observed in the parent complexes. Both the HOMO and LUMO are predominantly delocalized over the tricarbonyl-Mn and α-diimine metallacycle, with little participation from the phenyl ring, with the exception of MnIMP, the LUMO of which has a significant contribution from the phenyl moiety.

The UV−vis absorption spectra (Figure 2) are consistent with the nature of the frontier orbitals obtained from the
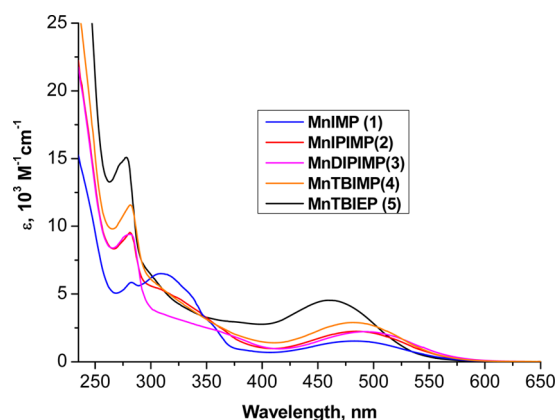

Figure 2. Electronic absorption spectra of the manganese complexes **1−5** studied in this work, in DCM at 293 K.

calculated data. The lowest energy absorption band for the complexes of the IMP subseries **1−4** occurs at approximately the same ca. 500 nm position. In contrast MnTBIEP (**5**) exhibits an absorption band with a maximum at a shorter wavelength, 460 nm, due to electron donation from the Me group which destabilizes the LUMO.

Cyclic Voltammetry. Electrochemical studies showed significant differences between the cathodic path of MnTBIEP (**5**) and those of the IMP subseries (**1−4**).

Under an N$_2$ atmosphere, [MnBr(CO)$_3$(TBIEP)] shows a single reduction wave at $E_{p,c}$ −1.53 V and an intense anodic wave at $E_{p,a}$ −1.3 V observed on the reverse anodic scan. This behavior is similar to that of [MnBr(CO)$_3$(^{i}Pr-DAB)] (^{i}Pr-DAB = 1,4-diisopropyl-1,4-diazabuta-1,3-diene),[8] which is reduced by an ECE mechanism. The initial one-electron reduction results in dissociation of the bromide to form a five-coordinate radical, [Mn(CO)$_3$(TBIEP)]$^\bullet$, which is concomitantly reduced to the five-coordinate anion [Mn(CO)$_3$(TBIEP)]$^-$ (reoxidized at −1.3 V) at the potential required for the reduction of [MnBr(CO)$_3$(TBIEP)]. A small anodic wave at −0.6 V is characteristic of oxidation of [Mn(CO)$_3$(TBIEP)]$_2$ formed in the course of the anodic path of the five-coordinate anion, and indicates that dimerization can still occur with R = CH$_3$. The dimer could also be produced in a reaction of [Mn(CO)$_3$(TBIEP)]$^-$ with neutral [MnBr(CO)$_3$(TBIEP)] on the cathodic scan, but the absence of a cathodic wave for reduction of [Mn(CO)$_3$(TBIEP)]$_2$ indicates that its reduction potential is too close to that of [MnBr(CO)$_3$(TBIEP)] for a separate reduction wave to be observed.

The CV traces of MnIMP obtained under a N$_2$ atmosphere show three cathodic reduction peaks at $E_{p,c}$ = −1.28, −1.41, and −1.54 V and a strong anodic peak at $E_{p,a}$ = −1.24 V. The first reduction at −1.28 V can be assigned to the cation [Mn(CO)$_3$(H$_2$O)(IMP)]$^+$; it is likely that the peak at −1.41 V is due to remaining nonhydrolyzed [MnBr(CO)$_3$(IMP)] or a solvent adduct,[11] while the −1.54 V wave corresponds to the reduction of the dimeric species (see also the IR spectroelectrochemical section below). The five-coordinate anion [Mn(CO)$_3$(IMP)]$^-$ is probably the reduction product at all three different cathodic waves (the parent complex [MnBr(CO)$_3$(IMP)], aquo complex, and the IMPMn−MnIMP

dimer), as evidenced by its anodic wave at $E_{p,a} = -1.24$ V on the reverse anodic scan (accompanied by the dimer oxidation above -0.5 V).

Over time a smaller cathodic wave emerges at $E_{p,c}$ -1.35 V, due to the aquo-coordinated cationic complex forming via hydrolysis of the parent Br complex (see Figures SI11 and SI12 in the Supporting Information). Under an atmosphere of CO_2 the anodic wave of $[Mn(CO)_3(TBIEP)]^-$ at -1.3 V disappears, and the profile of the CV also changes (Figure 3), with a broad
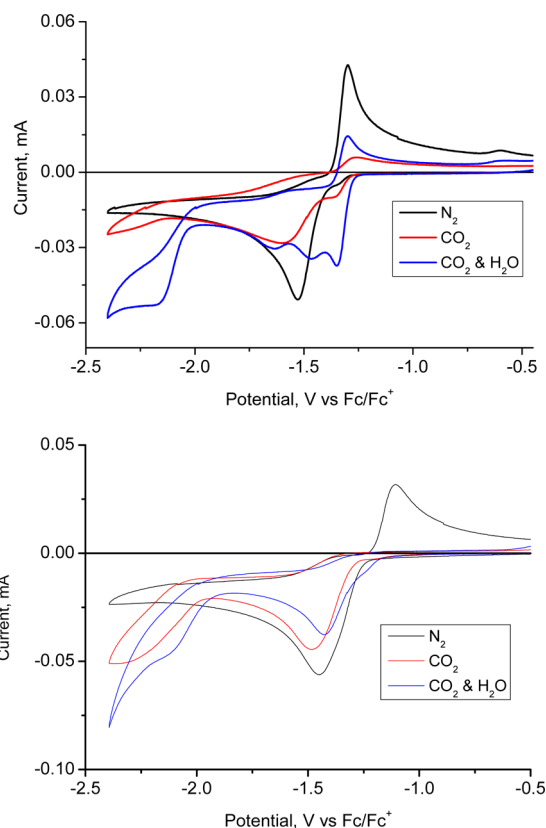
Figure 3. Cyclic voltammograms of 1 mM MnTBIEP (top panel) and MnTBIMP (bottom panel) in acetonitrile with 0.2 M $[Bu_4N][PF_6]$ as supporting electrolyte, under a N_2 atmosphere (black), CO_2 atmosphere (red), and CO_2 with 4.7% added water (blue) at a scan rate of 0.1 V s^{-1}.

cathodic wave of $[MnBr(CO)_3(TBIEP)]$ shifted slightly negatively, indicating an interaction with CO_2. However, similar to the case for Mn-bpy complexes,[2] catalytic reduction of CO_2 in the absence of a Brønsted acid was not observed (the small peak beginning around -2.18 V is due to a small amount of water entering the CV cell when it is being saturated with CO_2). Addition of 0.3 mL of water leads to significant current enhancement at -2.18 V, in line with what has been observed with $[MnBr(CO)_3(iPr-DAB)]$.[8]

Under a CO_2 atmosphere, the increased cathodic current is seen at ~-2.2 V for all complexes. We believe this is due to some amount of the bicarbonate complex being formed, likely due to traces of water in the CO_2 used.[33] When 10% water is added to the CO_2-saturated solution, a strong current enhancement is observed at -2.21 V. Importantly, CVs recorded under a N_2 atmosphere in acetonitrile in the presence of water do not show catalytic current enhancement (see Figures SI14−SI18 in the Supporting Information); thus, both

CO_2 and water are required for the current enhancement to be observed.

Under a CO_2 atmosphere, no anodic wave corresponding to reoxidation of the five-coordinate anion is observed for the least sterically hindered $[Mn(CO)_3(IMP)]^-$ (Figure 4) or for the

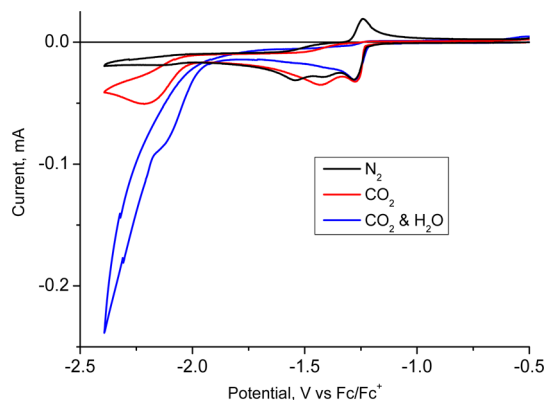**Figure 4.** Cyclic voltammograms of 1 mM MnIMP in acetonitrile with 0.2 M $[Bu_4N][PF_6]$ at a scan rate of 0.1 V s^{-1}, under an atmosphere of N_2 (black), CO_2 (red), and CO_2 with 4.7% H_2O (blue).

monosubstituted complexes **2** and **4**, a behavior indicative of a rapid reaction of the anion with CO_2. A diminished but clear anodic wave of $[Mn(CO)_3(TBIEP)]^-$ can be observed under a CO_2 vs a N_2 atmosphere (Figure 3), suggesting that $[Mn(CO)_3(TBIEP)]^-$ associates with CO_2 less efficiently. While, similarly to MnIPIMP, no anodic wave corresponding to $[Mn(CO)_3(TBIMP)]^-$ reoxidation under a CO_2 atmosphere could be observed, indicating that CO_2 association is rapid, the overall current enhancement for this complex is comparatively low, indicating lower efficiency at reducing CO_2, perhaps due to the bicarbonate intermediate somewhat preventing the recovery of the five-coordinate catalytic species.

Under N_2, reduction of $[MnBr(CO)_3(IPIMP)]$ is seen at $E_{p,c}$ -1.49 V, accompanied by a wave at $E_{p,c}$ -1.29 V, assigned to the cationic aqua complex $[Mn(CO)_3(H_2O)(IPIMP)]^+$ (Figure 5). As discussed above, upon addition of CO_2 the oxidation wave of the anion $[Mn(CO)_3(IPIMP)]^-$ is not observed, indicating a rapid reaction between the five-coordinate anion
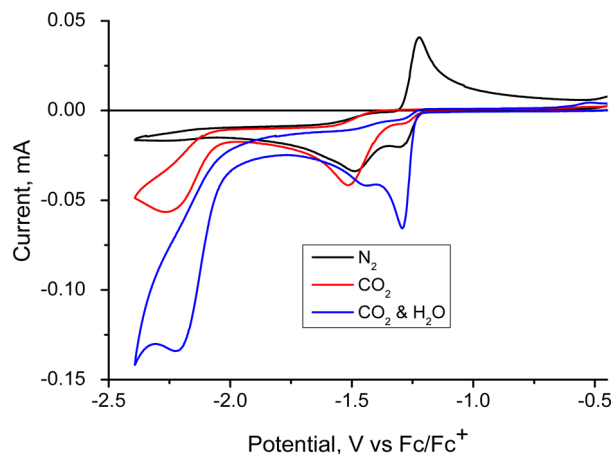
Figure 5. Cyclic voltammograms of 1 mM MnIPIMP in acetonitrile with 0.2 M $[Bu_4N][PF_6]$ at a scan rate of 0.1 V s^{-1}, under an atmosphere of N_2 (black), CO_2 (red), and CO_2 with 4.7% H_2O (blue).

and CO_2. Some current enhancement at -2.26 V is observed upon saturation with CO_2, which is enhanced greatly upon the addition of 0.3 mL of water (the current enhancement corresponds to the cathodic wave of the bicarbonate complex, identified in the IR spectra (vide infra): some catalysis occurs due to hydrolysis caused for example by residual water in the electrolyte or in the CO_2).

CV of MnTBIMP (Figure 3, bottom panel) is similar to that of MnIPIMP and MnTBIEP with a strong cathodic wave at -1.45 V. At ca. -2.28 V current enhancements ascribed to CO_2 reduction can be observed under CO_2 and CO_2 with added H_2O, though the i_{cat}/i_p values (Table SI1 in the Supporting Information) are somewhat lower in comparison to the other complexes studied here. Importantly, the anodic wave of the five-coordinate anion reoxidation is not detected for MnIPIMP and MnTBIMP but is clearly seen for slower reacting MnTBIEP and MnDIPIMP anions.

MnDIPIMP shows significant differences in the CV traces in comparison to the other complexes of the IMP subseries (Figure 6). Similarly to the IMP and IPIMP complexes, a
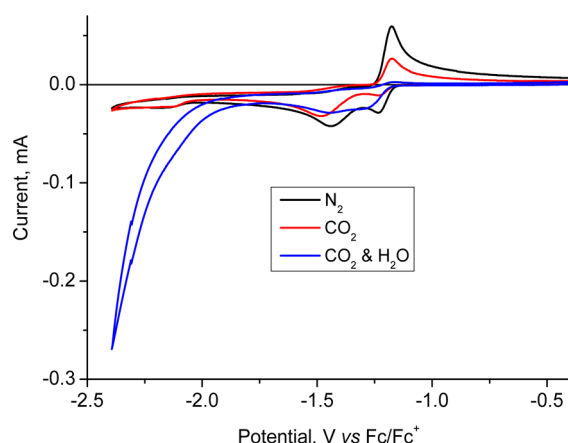
Figure 6. Cyclic voltammograms of 1 mM MnDIPIMP in acetonitrile with 0.2 M $[Bu_4N][PF_6]$ at a scan rate of 0.1 V s^{-1}, under an atmosphere of N_2 (black), CO_2 (red), and CO_2 with 4.7% H_2O (blue).

formation of an aqua cation complex ($[Mn(CO)_3(H_2O)(DIPIMP)]^+$) is observed in solution. However, upon saturation with CO_2 no additional processes (intermediate bicarbonate complex reduction) or current enhancement below -2 V is observed and the anodic peak due to oxidation of $[Mn(CO)_3(DIPIMP)]^-$ does not fully disappear. This suggests that the reduced complex is less prone to interact with CO_2, as would be expected due to the increased steric hindrance and structural rigidity of the complex arising from the two ^iPr substituents at the N-phenyl rings.

IR and UV−Vis Spectroelectrochemistry under an Inert Atmosphere. IR spectroscopy[20] is an ideal tool to monitor the cathodic processes in the studied complexes, due to presence of the carbonyl ligands as strong IR reporters. Table 2 gives the key experimental and calculated vibrational frequencies for the starting complexes and several relevant intermediate and dimer species. IR spectroelectrochemistry (IR-SEC) was used to probe the intermediates produced upon reduction and to monitor their presence during CO_2 reduction.

IR spectra of MnTBIEP (Figure 7) show, upon the first reduction, depletion of the parent ν(CO) bands, with new bands growing in at 1922 and 1898 cm^{-1} and a broad feature at
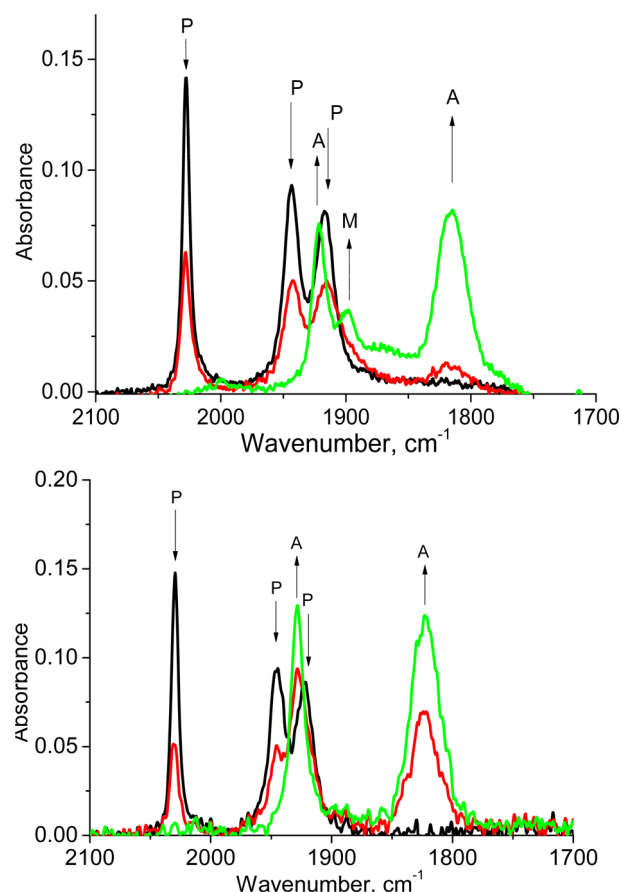
Figure 7. IR spectral changes accompanying in situ reduction of complexes in Ar-saturated acetonitrile/0.2 M $[Bu_4N][PF_6]$ within an OTTLE cell. (top) For MnTBIEP, a direct reduction of the parent complex (black line) to the five-coordinate anion (green line) is observed. :(P) $[MnBr(CO)_3(TBIEP)]$; (A) $[Mn(CO)_3(TBIEP)]^-$; (M) an unassigned side product. (bottom) For MnTBIMP, a direct reduction of the parent complex (black line) to the five-coordinate anion (green line) is observed: (P) $[MnBr(CO)_3(TBIMP)]$; (A) $[Mn(CO)_3(TBIMP)]^-$.

1814 cm^{-1}. The bands at 1922 and 1814 cm^{-1} can be assigned to the five-coordinate anion $[Mn(CO)_3(TBIEP)]^-$, an assignment supported by DFT calculations. The band at 1898 cm^{-1}, which grows in after the five-coordinate anion begins to form, could tentatively be attributed to a decomposition product. UV−vis spectroelectrochemistry (Figure SI13 in the Supporting Information) supports this notion, as only a band at ca. 570 nm has been detected, which corresponds to the five-coordinate anion. Differently from the MnIMP and MnIPIMP complexes (see below), there is no indication of dimer ($[Mn(CO)_3(TBIEP)]_2$) formation during the reduction of MnTBIEP on the time scale of the experiments performed.

MnTBIMP mirrors the behavior of MnTBIEP with the bands at 2029, 1945, and 1923 cm^{-1} corresponding to the parent complex being replaced concertedly with bands at 1928 and 1823 cm^{-1} corresponding to the five-coordinate anion, with no intermediate species being observed. This would suggest that the direct formation of the five-coordinate anion is due to the steric demands of the ^tBu group, since the mono-^iPr derivative **2** does exhibit dimer formation (Table 1).

The results of the IR-SEC study of MnIMP are shown in Figure 8. The first reduction of MnIMP in CH_3CN under an Ar atmosphere is accompanied by depletion of the parent IR bands
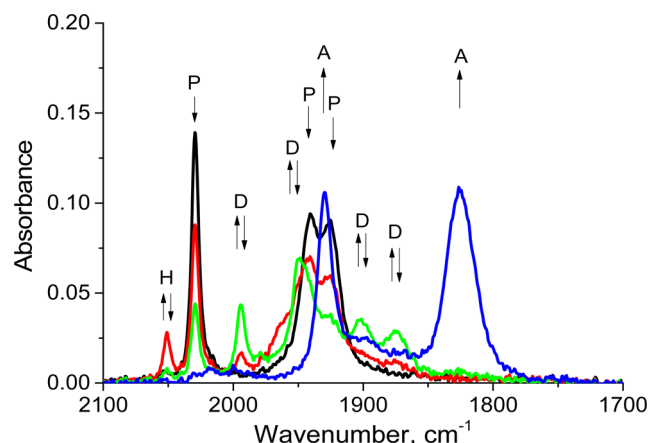
Figure 8. IR spectral changes accompanying in situ reduction of MnIMP in Ar-saturated acetonitrile/0.2 M [Bu$_4$N][PF$_6$] within an OTTLE cell. The parent complex [MnBr(CO)$_3$(IMP)] (P, black line), and aquo cation [Mn(CO)$_3$(H$_2$O)(IMP)]$^+$ (H, additional features in the red spectrum) are reduced to the dimer [MnBr(CO)$_3$(IMP)]$_2$ (D, green line) followed by reduction of the dimer to the five-coordinate anion [Mn(CO)$_3$(IMP)]$^-$ (A, blue line). The intermediate spectrum (red line) recorded between those of the parent complex and the dimer also shows the features of the aquo complex.
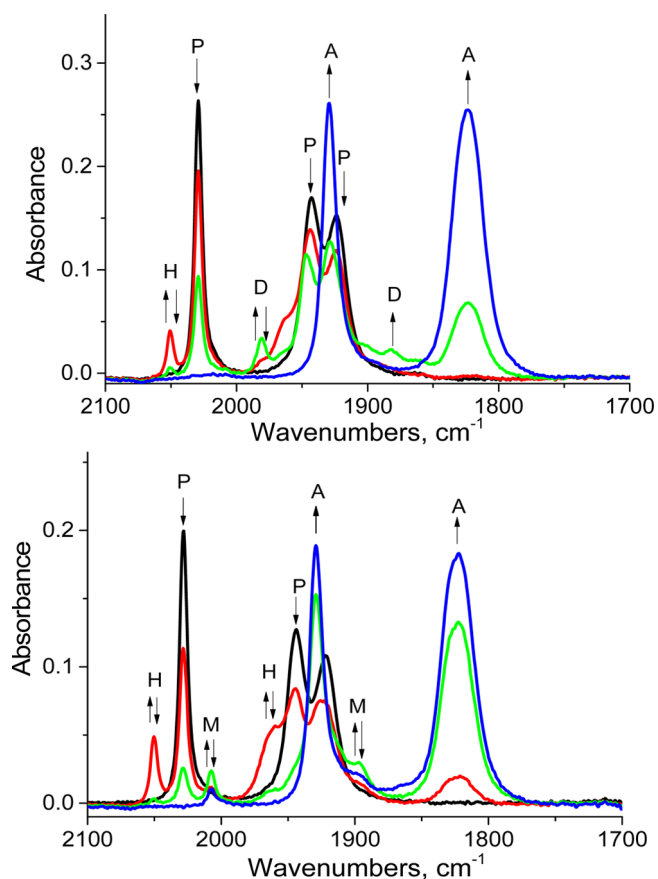
at 2029, 1941, and 1926 cm^{-1}. Simultaneously, the growth of new bands at 1994, 1949, 1902, and 1875 cm^{-1} is seen, which are characteristic of the Mn−Mn dimer[8,9,13,30] [Mn(CO)$_3$(IMP)]$_2$. Additionally, a peak at 2051 cm^{-1} grows in initially, which is assigned to the intermediate aqua cation [Mn(CO)$_3$(H$_2$O)(IMP)]$^+$ observed also by cyclic voltammetry. Further reduction of the dimer leads to formation of broad absorption bands at 1826 and 1930 cm^{-1}, once the formation of the dimer species is complete. These features are characteristic of the formation of the five-coordinate anion[8,9,13] [Mn(CO)$_3$(IMP)]$^-$. UV−vis spectroelectrochemistry performed in parallel with the IR-SEC experiment confirms the presence of both of these species (Figure SI14 in the Supporting Information) via the broad absorption band at ca. 800 nm (assigned to the dimer) and the intense absorption at ca. 675 nm (assigned to the five-coordinate anion).[8] All complexes in the IMP subseries exhibited a small transient peak at ca. 2050 cm^{-1} upon reduction. This is assigned to the aquo complex [Mn(CO)$_3$(H$_2$O)(IMP)]$^+$.

Differently from MnIMP, MnIPIMP showed concurrent formation of the dimer and the five-coordinate anion upon reduction of the parent complex (Figure 9, top). The introduction of the isopropyl substituent at the phenyl ring leads to the observation of a small amount of the five-coordinate anion [Mn(CO)$_3$(IPIMP)]$^-$ (absorbing at 1929 and 1824 cm^{-1}), which grows in alongside peaks indicative of dimer formation (1981, 1949, 1901, 1882, and 1862 cm^{-1}).

Importantly, the IR absorption bands, corresponding to both the dimer and the five-coordinate anion, grew in simultaneously. UV−vis spectroelectrochemistry confirmed the presence of both dimer and five-coordinate species in this case, as is evident from Figure SI13 in the Supporting Information).

In contrast, only the five-coordinate anion is detected already from the onset of the reduction of MnDIPIMP under the experimental conditions used. In this case, there is no evidence for the dimer formation during the reduction of the parent complex. As shown in Figure 9 (bottom), an intense peak at

Figure 9. IR spectral changes accompanying in situ reduction of the complexes in Ar-saturated acetonitrile/0.2 M [Bu$_4$N][PF$_6$] within an OTTLE cell. (top) MnIPIMP, with concurrent formation of a dimer and a five-coordinate anion on reduction of the parent complex being observed: (P) [MnBr(CO)$_3$(IPIMP)]; (D) [Mn(CO)$_3$(IPIMP)]$_2$; (A) [Mn(CO)$_3$(IPIMP)]$^-$; (H) [Mn(CO)$_3$(H$_2$O)(IPIMP)]$^+$. (bottom) MnDIPIMP, with reduction of the parent complex to a five-coordinate anion being observed: (P) [MnBr(CO)$_3$(DIPIMP)]; (A) [Mn(CO)$_3$(DIPIMP)]$^-$; (H) [Mn(CO)$_3$(H$_2$O)(DIPIMP)]$^+$; (M) [Mn(CO)$_3$(MeCN)(DIPIMP)]$^•$.

1823 cm^{-1}, assigned to the five-coordinate anion, grew in, followed closely by smaller peaks at 2007 and 1899 cm^{-1}. The second peak assigned to the five-coordinate anion at 1929 cm^{-1} was masked by the absorption of the parent complex at the beginning of the reduction process. We tentatively assign the peaks at 2007/1899 cm^{-1} to the solvent-coordinated radical species [Mn(CO)$_3$(MeCN)(DIPIMP)]$^•$, in analogy with [Re(CO)$_3$(PrCN)(^{i}Pr-PyCa)][17] (^{i}Pr-PyCa = (isopropylimino)-pyridine; PrCN = butyronitrile) which shows ν(CO) bands at 2005 and 1885 (br) cm^{-1}. Further, since the anodic wave of the dimer oxidation is not observed in the CV of MnDIPIMP, but a 1e reduced radical species is observed in IR-SEC, it is evident that the DIPIMP ligand prevents dimerization.

MnTBIMP shows behavior intermediate to that of MnTBIEP and MnIPIMP: similarly to MnTBIEP, the ^{t}Bu substituent prevent dimer formation upon reduction. However, differently from MnTBIEP, and similar to MnIPIMP, a rapid reaction with CO$_2$ takes place, which in the case of MnTBIEP is considerably slowed by the R = Me group. It is important to note that if Mn−Mn dimer is reduced at the same or even less negative potentials than that of the parent complex, it will not be detected in the studies.[9] Thus, the comments above

regarding the absence of dimer formation only relate to the Br complexes studied here. Substituting Br$^-$ with a different group, which would lead to the parent complex being reduced at less negative potentials, may permit detection of these species. Five-coordinate complex formation appears to correlate with a less negative first reduction potential (see Table 3). A comparable

Table 3. Cathodic Potentials (V, vs Fc/Fc$^+$) of the Parent Complexes [MnBr(CO)$_3$(IP)] (1 mM, Acetonitrile, 0.2 M [Bu$_4$N][PF$_6$]) and Corresponding Cationic Mn Aquo Derivatives Formed in Situ by Partial Hydrolysis

complex	$E_{p,c}$	catalytic potential[b]
[MnBr(CO)$_3$(IMP)] (1)	−1.41, −1.54[a]	−2.21
[Mn(CO)$_3$(H$_2$O)(IMP)]$^+$	−1.28	
[MnBr(CO)$_3$(IPIMP)] (2)	−1.49	−2.26
[Mn(CO)$_3$(H$_2$O)(IPIMP)]$^+$	−1.29	
[MnBr(CO)$_3$(DIPIMP)] (3)	−1.44	−2.16
[Mn(CO)$_3$(H$_2$O)(DIPIMP)]$^+$	−1.23	
[MnBr(CO)$_3$(TBIMP)] (4)	−1.45	∼−2.28
[MnBr(CO)$_3$(TBIEP)] (5)	−1.53	−2.18
[Mn(CO)$_3$(H$_2$O) (TBIEP)]$^+$	−1.35	

[a]This process probably corresponds to a reduction of the dimer. [b]Largely coinciding with the reduction of a bicarbonate complex (see the spectroelectrochemical section).

correlation was found for Mn-R-DAB complexes and sterically hindered 2,2′-bipyridines already reported in the literature. These complexes also exhibit less negative first reduction potentials in comparison to their less sterically hindered counterparts and form five-coordinate anions directly upon reduction.[8,25]

IR and UV−Vis Spectroelectrochemistry under a CO$_2$ Atmosphere. Electrochemical behavior under a CO$_2$ atmosphere is vastly different from that under a N$_2$ or Ar atmosphere. The electrocatalytic reduction of CO$_2$ with the four Mn complexes can be described in terms of three different types of behavior, largely controlled by the steric hindrance of the active imino C═N bond. MnIMP and MnIPIMP are relatively unhindered, and the catalytic behaviors are almost identical. The initial reduction of parent and/or the cationic aqua complex results in the formation of the two-electron-reduced five-coordinate anion that reacts efficiently with CO$_2$; no dimer is observed during the reduction of MnIMP (Figure 10) or MnIPIMP (Figure 11).

The catalytic process at the initial cathodic wave is, however, inhibited by the rapid formation of a stable bicarbonate complex, absorbing at 2036, 1940, 1924, and 1671 cm^{-1} for the IPIMP species, in line with the reports for sterically hindered Mn-mesityl-bipyridine[25] complexes and Mn-R-DAB complexes.[8] A further negative potential shift of ca. 0.7 V is needed to reduce the bicarbonate complex, resulting in the recovery of the five-coordinate anion that triggers the catalytic conversion of CO$_2$.

For the nonhindered IMP and IPIMP ligands the five-coordinate anion reacts rapidly and is not observed in the IR spectra on this time scale (for IMP) and only at a low concentration (for IPIMP). The production of CO in the thin solution layer results in the displacement of the α-diimine ligand in the five-coordinate anion, forming the pentacarbonyl species [Mn(CO)$_5$]$^-$ clearly seen in the IR spectra via the growth of bands at 1897 and 1865 cm^{-1} (species C in Figures 10−13). Remarkably, in these two cases only a comparatively
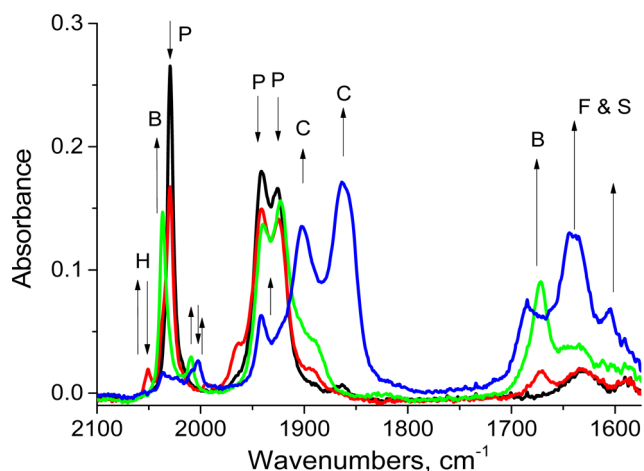
Figure 10. IR spectral changes accompanying in situ reduction of MnIMP ([MnBr(CO)$_3$(IMP)]) in CO$_2$-saturated acetonitrile/0.2 M [Bu$_4$N][PF$_6$] within an OTTLE cell: (P) [MnBr(CO)$_3$(IMP)]; (B) [Mn(CO)$_3$(IMP)(η^1-OCO$_2$H)]; (C) [Mn(CO)$_5$]$^-$; (H) [Mn(CO)$_3$(H$_2$O)(IMP)]$^+$; (F and S) free bicarbonate (OCO$_2$H$^-$) and subordinate formate (OCHO$^-$) accompanying the catalytic reduction of CO$_2$ to CO.
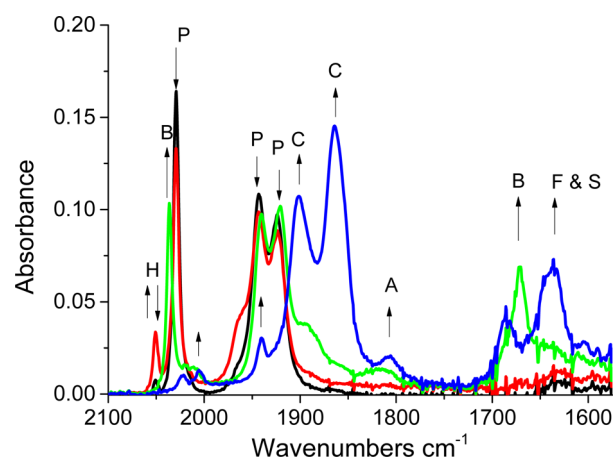
Figure 11. IR spectral changes accompanying in situ reduction of MnIPIMP ([MnBr(CO)$_3$(IPIMP)]) in CO$_2$-saturated acetonitrile/0.2 M [Bu$_4$N][PF$_6$] in an OTTLE cell: (P) [MnBr(CO)$_3$(IPIMP)]; (A) [Mn(CO)$_3$(IPIMP)]$^-$; (B) [Mn(CO)$_3$(IPIMP)(η^1-OCO$_2$H)]; (C) [Mn(CO)$_5$]$^-$; (H) [Mn(CO)$_3$(H$_2$O)(IPIMP)]$^+$; (F and S) free bicarbonate (OCO$_2$H$^-$) and subordinate formate (OCHO$^-$) accompanying the catalytic reduction of CO$_2$ to CO.

small amount of free bicarbonate or free formate (1685, 1638, and 1604 cm^{-1} for the IPIMP species) relative to [Mn(CO)$_5$]$^-$ is observed, marking the high catalytic efficiency toward CO production.

Upon reduction of the more C═N hindered DIPIMP complex, the five-coordinate anion formed does not react with CO$_2$ efficiently and a metastable population of the anionic five-coordinate MnDIPIMP species [Mn(CO)$_3$(DIPIMP)]$^-$ is detected even under a high excess of CO$_2$. Interestingly, and differently from the other complexes in the Mn-IP series, the formation of a bicarbonate complex is only detected at the potential corresponding to the reduction of CO$_2$-associated species at around −2 V vs Fc/Fc$^+$, while on prior coordination of CO$_2$ to the five-coordinate anion at the parent MnDIPIMP cathodic wave no bicarbonate ligand signature is detected. At the catalytic potential where the bicarbonate complex is
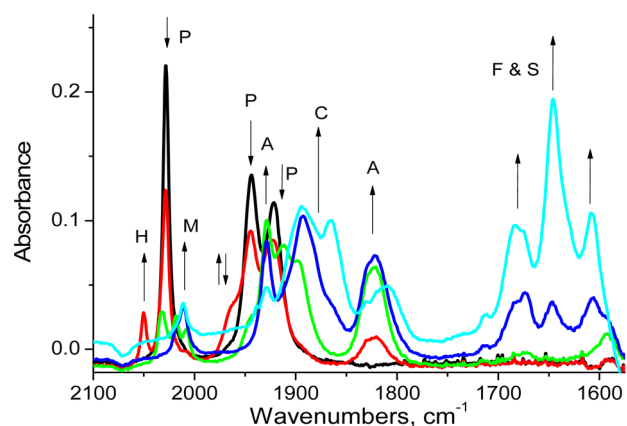
Figure 12. IR spectral changes accompanying in situ reduction of MnDIPIMP in CO_2-saturated acetonitrile/0.2 M $[Bu_4N][PF_6]$ within an OTTLE cell: (P) $[MnBr(CO)_3(DIPIMP)]$; (A) $[Mn(CO)_3(DIPIMP)]^-$; (B) $[Mn(CO)_3(DIPIMP)(\eta^1\text{-}OCO_2H)]$; (H) aqua complex $[Mn(CO)_3(H_2O)(DIPIMP)]^+$; (C) $[Mn(CO)_5]^-$; (M) $[Mn(CO)_3(MeCN)(DIPIMP)]^\bullet$; (F and S) free bicarbonate (OCO_2H^-) and subordinate formate $(OCHO^-)$.

reduced, the conversion of CO_2 to CO is also inefficient. A high concentration of the five-coordinate anion is still seen, converting slowly to $[Mn(CO)_5]^-$ when the concentration of CO increases; at the same time the production of free bicarbonate (and free formate) is much higher in comparison to the MnIMP and MnIPIMP cases, marking the low catalytic efficiency toward CO production. Notably, the lower CO-stretching band of $[Mn(CO)_3(DIPIMP)]^-$ becomes shifted from its standard position (1829/1822 cm^{-1}) to lower energy (ca. 1810 cm^{-1}) at the advanced stage of the catalytic conversion. This shift may indicate the presence of an observable adduct of the five-coordinate anion, most likely with CO_2 or formate (over the Mn−N≡C bond). In this context it is interesting to note that the related Re-IP complex[37] forms the carbonate complex in two 1e-reduction steps, via a direct coordination to the Re center, without C≡N being directly involved.

In the case of MnTBIEP the imino C≡N bond is hindered both at the carbon atom via the methyl group and by the *tert*-butyl group on the phenyl moiety. There are similarities with but also differences from the hindered DIPIMP complex, which does not have a hindering group at the C atom of the imino C≡N moiety. Upon reduction of the parent complex in CO_2-saturated acetonitrile the five-coordinate anion $[Mn(CO)_3(TBIEP)]^-$ coordinates CO_2, forming the bicarbonate complex readily (similar to IMP and IPIMP) with the characteristic IR absorption band at 1673 cm^{-1}.[8,30]

A small amount of the five-coordinate anion $[Mn(CO)_3(TBIEP)]^-$ is observed in the initial step. Lowering the potential to around −1.5 V vs Fc/Fc$^+$ results in catalytic conversion of the bicarbonate complex; however, similar to MnDIPIMP this conversion is not efficient in comparison with MnIMP and MnIPIMP. This is shown via the slower growth of $[Mn(CO)_5]^-$ in comparison to IPIMP and the greater quantities of free bicarbonate produced. As with MnDIPIMP the five-coordinate anion "adduct" form is observed with the lower energy CO-stretching band shifted to a lower wavenumber (from 1814 to 1803 cm^{-1}). Thus, hindering the imine C atom does not affect adduct formation between CO_2 and $[Mn(CO)_3(TBIEP)]^-$.
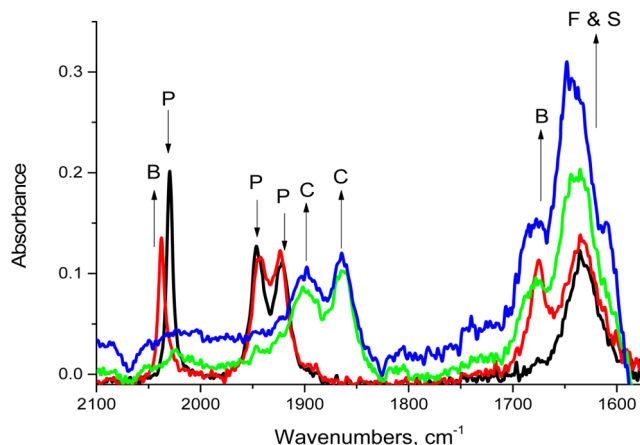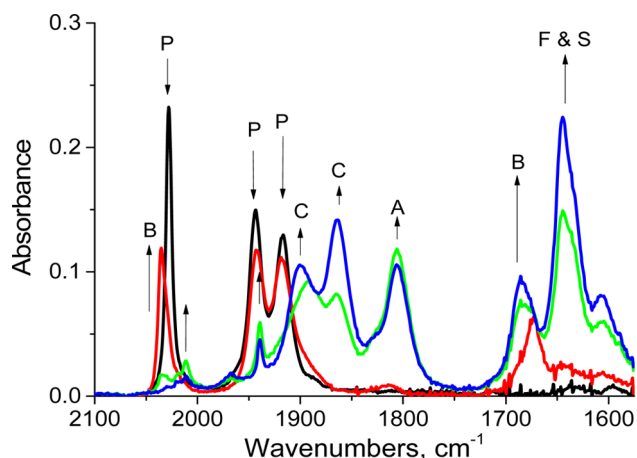

Figure 13. IR spectral changes accompanying in situ reduction of complexes in CO_2-saturated acetonitrile/0.2 M $[Bu_4N][PF_6]$ within an OTTLE cell. (top) For MnTBIEP: (P) $[MnBr(CO)_3(TBIEP)]$; (A) $[Mn(CO)_3(TBIEP)]^-$; (B) $[Mn(CO)_3(TBIEP)(\eta^1\text{-}OCO_2H)]$; (C) $[Mn(CO)_5]^-$; (F and S) free bicarbonate (OCO_2H^-) and formate $(OCHO^-)$ accompanying the catalytic reduction of CO_2 to CO. (bottom) For MnTBIMP: (P) $[MnBr(CO)_3(TBIMP)]$; (B) $[Mn(CO)_3(TBIMP)(\eta^1\text{-}OCO_2H)]$; (C) $[Mn(CO)_5]^-$; (F and S) free bicarbonate (OCO_2H^-) and formate $(OCHO^-)$ accompanying the catalytic reduction of CO_2 to CO.

However, at the negative potentials where the bicarbonate complex is reduced (recovering the catalytic five-coordinate anion) the hindrance provided by the methyl and *tert*-butyl groups also negatively affects the catalytic formation of CO_2 to CO (as evidenced by large amounts of free bicarbonate and slow formation of $[Mn(CO)_5]^-$ at lower CO concentration). It is not very clear whether this greater hindrance is due directly to the presence of the methyl group on the C position or whether this is due to the *tert*-butyl group inhibiting rotation of the phenyl moiety and preventing the five-coordinate anion from adopting a more suitable (pyramidal) geometry for CO_2 association.

Again, MnTBIMP behaves in a fashion similar to that of MnTBIEP. Upon reduction the parent complex rapidly associates CO_2, forming the bicarbonate complex; as the reduction potential is lowered further, the bicarbonate complex is reduced, forming CO which is able to displace the TBIMP and forming $[Mn(CO)_5]^-$. One important difference is that significantly less (if any) five-coordinate anion is observed in the presence of CO_2 than was the case with both MnTBIEP

and MnDIPIMP. This suggests that ^{t}Bu is not as sterically demanding as two ^{i}Pr groups in these systems, as CO_2 is still able to coordinate.

Estimation of Electrocatalytic Activity toward CO Production using Gas Chromatography. The CO concentration as a function of time in the course of controlled potential electrolysis estimated by GC analysis of the headspace of the electrolysis cell shows a gradual buildup of CO in the course of the electrolysis (Figure SI19 in the Supporting Information). A comparison with the performance of [MnBr-$(CO)_3(bpy)$] catalyst investigated under identical conditions (see Figure S19) shows that the efficiency of CO production for the new catalysts **1**−**5** is comparable to that of [MnBr$(CO)_3(bpy)$], with the least sterically hindered MnIMP complex being somewhat more efficient. Due to the large volumes used in the experiment, considerable secondary processes occur during bulk electrolysis, manifested in the loss of the initial intense yellow-red color of the solution as the reaction progressed, which was concomitant with an increase in current toward the end of the electrolysis. These deviations from an ideal behavior suggest that, as CO_2 is depleted in solution, competing catalyst degradation pathways begin to occur, precluding reliable estimates of efficiencies.

Estimation of efficiency from the CV data was done by the relative i_{cat}/i_p values (Table S1 in the Supporting Information) following the method described in refs 4 and 7. Comparing the current values detected in the CV at −2.24 V (vs Fc/Fc$^+$) recorded under a CO_2 and N_2 atmosphere in acetonitrile/water also shows that the performances of **1**−**5** are comparable to one another and are comparable to that of [Mn$(CO)_3$(bpy)Br], at 30−60% efficiency. It is important that the most sterically protected complexes, MnDIPIMP and MnTBIEP, seem to be performing better as far as i_{cat}/i_p values are concerned but that the least sterically hindered complex, MnIMP, is the most efficient in the series. These observations are different from the observation of MnTBIMP producing more CO than [Mn-$(bpy)(CO)_3$Br] in the bulk electrolysis/GC experiments. While these data can only be considered in relative terms, they do show the potential of these complexes to act as a test bed for optimizing steric vs electronic effects in CO_2 reduction, whereby the thermodynamic factors, the rate of CO_2 coordination, and the rate of decomposition of catalyst precursor species need to be balanced.
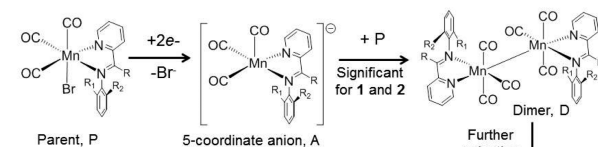
The main transformation pathways of **1**−**5** upon reduction under an inert atmosphere, and under an atmosphere of CO_2, are summarized schematically in Figure 14.

■ CONCLUSIONS

A series of Mn(I) tricarbonyl electrocatalysts for CO_2 reduction which employ, for the first time, asymmetric α-diimine ligands, imino-pyridines, has been developed, and their catalytic activity has been confirmed and evaluated in detail.

We have demonstrated through conventional and thin-layer cyclic voltammetry, UV−vis and IR spectroscop, and DFT computational analysis the π decoupling of the phenyl from the Mn(pyridine-CCN) metallacycle. The practical effect of this feature is the ability to disentangle steric and electronic effects of the α-diimine ligand on the catalytic properties. Until now, introduction of sterically bulky groups, which are also typically electron donating, was coming at the price of an increased overpotential required for CO_2 reduction. The use of an asymmetric α-diimine has allowed us to probe the effect of adding ever greater sterically demanding groups without much
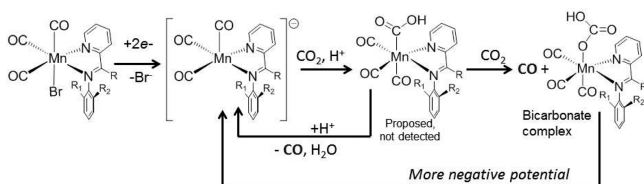
Figure 14. Main transformation pathways of **1**−**5** upon reduction under (a) an inert atmosphere and (b) an atmosphere of CO_2. **A** is detected for **3** only due to the comparatively slower reaction of [**3**]$^-$ with CO_2.

change in the catalytic potential. We have demonstrated that a systematic increase in the steric hindrance of the R_1 and R_2 groups in the IMP subseries results in the switch of the nature of the first reduction product detected on the time scale of the experiment under an inert gas atmosphere, from a dimer to a five-coordinate anion, at a very similar reduction potential. In the absence of sterically hindering groups on the phenyl ring, MnIMP, a dimer is formed, while increasing the steric hindrance by adding ^{i}Pr groups to the R_1 and R_2 positions (MnDIPIMP) resulted in direct formation of the five-coordinate anion, in line with prior observations for similar sterically hindered ligands.[23,26] MnIPIMP (in which case the dimer may be reduced at the parent cathodic wave due to slightly negatively shifted reduction potential vs that for MnIMP) exhibited behavior intermediate to that of MnIMP and MnDIPIMP with both the dimer and the five-coordinate anion observed to be formed concurrently. MnTBIMP and MnTBIEP both formed the five-coordinate anion directly upon reduction of the parent complex.

Under a CO_2 atmosphere, all of the complexes reduce CO_2 to CO. The buildup of CO in the thin-layer spectroelectrochemical cell resulted in the displacement of the α-diimine ligand, forming [Mn$(CO)_5$]$^-$. The complex containing the most sterically demanding ligand, DIPIMP, is as anticipated least susceptible to α-diimine displacement with CO, forming exclusively the five-coordinate anion upon the first reduction; it also has the least propensity to coordinate CO_2, resulting in a considerable buildup of the concentration of the five-coordinate anion. An intermediate formation of the bicarbonate is also likely, as a band at 1686 cm^{-1} is present at intermediate times. Of particular interest is that the least sterically hindered complex, MnIMP, seemed to form a CO_2-associated complex directly upon the first reduction, with no significant formation of the dimer being observed on the time scale of the experiment. This behavior is similar to that reported for the symmetric nonaromatic Mn-R-DAB (R = alkyl) compounds.[8,30] The formation of a stable bicarbonate complex, either through the coordination to the metal center or via the imino C=N bond,[23,37] leads to the need for increased overpotential. From that point of view, the steric hindering (protection) of the metal center/the imino C=N bond in the Mn(IP) complexes is advantageous, as it disfavors the Mn−Mn dimerization (when

MnIMP is compared with MnDIPIMP). However, such steric crowding also slows the catalytic conversion of CO_2 to CO at the negative overpotentials, as can be seen in the GC data and from the i_{cat}/i_p values. A difference in the reactivity of MnTBIMP and MnTBIEP, where no dimer formation has been detected for either of the complexes in the IR-SEC experiments but where MnTBIEP exhibits slower CO_2 conversion due to R = CH_3, alters the HOMO−LUMO gap in comparison to the IMP series as well as introduces additional steric bulk, further supporting the notion that it is possible to separate steric and electronic factors to a large extent. Balancing these factors by careful ligand design may lead to the optimal solution.

The new family of CO_2 reduction catalysts presents an exciting platform for versatile and relatively independent tuning of steric and electronic properties, offering a far greater tunability in comparison to catalysts with aromatic bpy-based or nonaromatic R-DAB-based ligands and abundant options to refine and optimize Mn tricarbonyl CO_2 reduction catalysts.

■ ASSOCIATED CONTENT

Ⓢ Supporting Information

The Supporting Information is available free of charge on the ACS Publications website at DOI: 10.1021/acs.inorg-chem.6b01477.

Calculated frontier orbitals from HOMO-3 to LUMO+3 for all studied complexes, complete CV measurements, control experiments, crystallographic data, and ^1H NMR spectra of the new complexes (PDF)

Crystallographic data (CIF)

Crystallographic data (CIF)

■ AUTHOR INFORMATION

Corresponding Authors

*E-mail for F.H.: F.Hartl@reading.ac.uk.
*E-mail for J.A.W.: Julia.Weinstein@sheffield.ac.uk.

ORCID Ⓞ

Anthony J. H. M. Meijer: 0000-0003-4803-3488
Julia A. Weinstein: 0000-0001-6883-072X

Notes

The authors declare no competing financial interest.

■ REFERENCES

(1) Morris, A. J.; Meyer, G. J.; Fujita, E. Molecular Approaches to Photocatalytic Reduction of Carbon Dioxide for Solar Fuels. *Acc. Chem. Res.* **2009**, *42*, 1983−1994.

(2) Bourrez, M.; Molton, F.; Chardon-Noblat, S.; Deronzier, A. [Mn(bipyridyl) (CO)$_3$Br]: An Abundant Metal Carbonyl Complex as Efficient Electrocatalyst for CO2 Reduction. *Angew. Chem., Int. Ed.* **2011**, *50*, 9903−9906.

(3) Hawecker, J.; Lehn, J.-M.; Ziessel, R. Electrocatalytic Reduction of Carbon Dioxide Mediated by Re(bipy) (CO)$_3$Cl (bipy = 2,2′-bipyridine). *J. Chem. Soc., Chem. Commun.* **1984**, 328−330.

(4) Smieja, J. M.; Benson, E. E.; Kumar, B.; Grice, K. A.; Seu, C. S.; Miller, A. J. M.; Mayer, J. M.; Kubiak, C. P. Kinetic and structural studies, origins of selectivity, and interfacial charge transfer in the artificial photosynthesis of CO. *Proc. Natl. Acad. Sci. U. S. A.* **2012**, *109*, 15646−15650.

(5) Grice, K. A.; Kubiak, C. P.; Aresta, M. Recent Studies of Rhenium and Manganese Bipyridine Carbonyl Catalysts for the Electrochemical Reduction of CO$_2$. *Adv. Inorg. Chem.* **2014**, *66*, 163−188. Aresta, M.; Dibenedetto, A.; Angelini, A. Converting ″Exhaust″ Carbon into ″Working″ Carbon. *Adv. Inorg. Chem.* **2014**, *66*, 259−288.

(6) Wong, K.; Chung, W.; Lau, C. The effect of weak Brönsted acids on the electrocatalytic reduction of carbon dioxide by a rhenium tricarbonyl bipyridyl complex. *J. Electroanal. Chem.* **1998**, *453*, 161−170.

(7) Smieja, J. M.; Sampson, M. D.; Grice, K. A.; Benson, E. E.; Froehlich, J. D.; Kubiak, C. P. Manganese as a Substitute for Rhenium in CO_2 Reduction Catalysts: The Importance of Acids. *Inorg. Chem.* **2013**, *52*, 2484−2491.

(8) Zeng, Q.; Tory, J.; Hartl, F. Electrocatalytic Reduction of Carbon Dioxide with a Manganese(I) Tricarbonyl Complex Containing a Nonaromatic α-Diimine Ligand. *Organometallics* **2014**, *33*, 5002−5008.

(9) Rossenaar, B. D.; Hartl, F.; Stufkens, D. J.; Amatore, C.; Maisonhaute, E.; Verpeaux, J.-N. Electrochemical and IR/UV-Vis Spectroelectrochemical Studies of fac-[Mn(X) (CO)$_3$(^{i}Pr-DAB)]^n (n = 0, X = Br, Me, Bz; n = +1, X = THF, MeCN, nPrCN, P(OMe)$_3$; iPr-DAB = 1,4-Diisopropyl-1,4-diaza-1,3-butadiene) at Variable Temperatures: Relation between Electrochemical and Photochemical Generation of [Mn(CO)$_3$(α-diimine)]$^-$. *Organometallics* **1997**, *16*, 4675−4685.

(10) Grills, D. C.; Farrington, J. A.; Layne, B. H.; Lymar, S. V.; Mello, B. A.; Preses, J. M.; Wishart, J. F. Mechanism of the Formation of a Mn-Based CO_2 Reduction Catalyst Revealed by Pulse Radiolysis with Time-Resolved Infrared Detection. *J. Am. Chem. Soc.* **2014**, *136*, 5563−5566.

(11) Johnson, F. P. A.; George, M. W.; Hartl, F.; Turner, J. J. Electrocatalytic Reduction of CO_2 Using the Complexes [Re(bipy) (CO)$_3$L]^n (n = + 1, L = P(OEt)$_3$, CH$_3$CN; n = 0, L = Cl$^-$, Otf$^-$; bpy = 2,2′-Bipyridine; Otf$^-$ = CF$_3$SO$_3$) as Catalyst Precursors: Infrared Spectroelectrochemical Investigation. *Organometallics* **1996**, *15*, 3374−3387.

(12) Smieja, J. M.; Kubiak, C. P. Re(bipy-^{t}Bu)(CO)$_3$Cl-improved Catalytic Activity for Reduction of Carbon Dioxide: IR-Spectroelectrochemical and Mechanistic Studies. *Inorg. Chem.* **2010**, *49*, 9283−9289.

(13) Machan, C. W.; Sampson, M. D.; Chabolla, S. A.; Dang, T.; Kubiak, P. Developing a Mechanistic Understanding of Molecular Electrocatalysts for CO_2 Reduction using Infrared Spectroelectrochemistry. *Organometallics* **2014**, *33*, 4550−4559.

(14) Cabeza, J. A.; Garcia-Alvarez, P.; Gobetto, R.; Gonzalez-Alvarez, L.; Nervi, C.; Perez-Carreno, E.; Polo, D. [MnBrL(CO)$_4$] (L = Amidinatogermylene): Reductive Dimerization, Carbonyl Substitution, and Hydrolysis Reactions. *Organometallics* **2016**, *35*, 1761−1770.

(15) Machan, C. W.; Stanton, C. J.; Vandezande, J. E.; Majetich, G. F.; Schaefer, H. F.; Kubiak, C. P.; Agarwal, J. Electrocatalytic Reduction of Carbon Dioxide by Mn(CN)(2,2′-bipyridine) (CO)$_3$: CN Coordination Alters Mechanism. *Inorg. Chem.* **2015**, *54*, 8849−8856.

(16) Sieh, D.; Kubiak, C. P. A Series of Diamagnetic Pyridine Monoimine Rhenium Complexes with Different Degrees of Metal-to-Ligand Charge Transfer: Correlating ^{13}C NMR Chemical Shifts with Bond Lengths in Redox-Active Ligands. *Chem. - Eur. J.* **2016**, *22*, 10638−10650.

(17) Riplinger, C.; Sampson, M. D.; Ritzmann, A. M.; Kubiak, C. P.; Carter, E. A. Mechanistic Contrasts between Manganese and Rhenium

Bipyridine Electrocatalysts for the Reduction of Carbon Dioxide. *J. Am. Chem. Soc.* **2014**, *136*, 16285−16298.

(18) Franco, F.; Cometto, C.; Ferrero Vallana, F.; Sordello, F.; Priola, E.; Minero, C.; Nervi, C.; Gobetto, R. A local proton source in a [Mn(bpy-R) (CO)₃Br]-type redox catalyst enables CO₂ reduction even in the absence of Brønsted acids. *Chem. Commun.* **2014**, *50*, 14670−14673.

(19) Bourrez, M.; Orio, M.; Molton, F.; Vezin, H.; Duboc, C.; Deronzier, A.; Chardon-Noblat, S. Pulsed-EPR Evidence of a Manganese(II) Hydroxycarbonyl Intermediate in the Electrocatalytic Reduction of Carbon Dioxide by a Manganese Bipyridyl Derivative. *Angew. Chem., Int. Ed.* **2014**, *53*, 240−243.

(20) Sullivan, B. P.; Bolinger, C. M.; Conrad, D.; Vining, W. J.; Meyer, T. J. One- and Two-electron Pathways in the Electrocatalytic Reduction of CO₂ by *fac*-Re(bpy) (CO)₃Cl (bpy = 2,2′-bipyridine). *J. Chem. Soc., Chem. Commun.* **1985**, 1414−1416.

(21) Stor, G. J.; Hartl, F.; van Outersterp, J. W. M.; Stufkens, D. J. Spectroelectrochemical (IR, UV/Vis) Determination of the Reduction Pathways for a Series of [Re(CO)₃(α-diimine)L′]⁰/⁺ (L′ = Halide, Otf⁻, THF, MeCN, *n*-PrCN, PPh₃, P(OMe)₃) Complexes. *Organometallics* **1995**, *14*, 1115−1131.

(22) Walsh, J. J.; Smith, C. L.; Neri, G.; Whitehead, G. F. S.; Robertson, C. M.; Cowan, A. J. Improving the efficiency of electrochemical CO₂ reduction using immobilized manganese complexes. *Faraday Discuss.* **2015**, *183*, 147−160.

(23) Stor, G. J.; Morrison, S. L.; Stufkens, D. J.; Oskam, A. The Remarkable Photochemistry of *fac*-XMn(CO)₃(α-diimine) (X = Halide): Formation of Mn₂(CO)₆(α-diimine)₂ via the *mer* Isomer and Photocatalytic Substitution of X⁻ in the Presence of PR₃. *Organometallics* **1994**, *13*, 2641−2650.

(24) Sampson, M. D.; Kubiak, C. P. Electrocatalytic Dihydrogen Production by an Earth-Abundant Manganese Bipyridine Catalyst. *Inorg. Chem.* **2015**, *54*, 6674−6676.

(25) Sampson, M. D.; Nguyen, A. D.; Grice, K. A.; Moore, C. E.; Rheingold, A. L.; Kubiak, C. P. Manganese Catalysts with Bulky Bipyridine Ligands for the Electrocatalytic Reduction of Carbon Dioxide: Eliminating Dimerization and Altering Catalysis. *J. Am. Chem. Soc.* **2014**, *136*, 5460−5471.

(26) Agarwal, J.; Shaw, T. W.; Stanton, C. J., III; Majetich, G. F.; Bocarsly, A. B.; Schaefer, H. F., III NHC-Containing Manganese(I) Electrocatalysts for the Two-Electron Reduction of CO₂. *Angew. Chem.* **2014**, *126*, 5252−5255.

(27) Costentin, C.; Robert, M.; Savéant, J.-M. Catalysis of the electrochemical reduction of carbon dioxide. *Chem. Soc. Rev.* **2013**, *42*, 2423−2436.

(28) Sampson, M. D.; Kubiak, C. P. Manganese Electrocatalysts with Bulky Bipyridine Ligands: Utilizing Lewis Acids To Promote Carbon Dioxide Reduction at Low Overpotentials. *J. Am. Chem. Soc.* **2016**, *138*, 1386−1393.

(29) Lam, Y. C.; Nielsen, R. J.; Gray, H. B.; Goddard, W. A. A Mn Bipyrimidine Catalyst Predicted To Reduce CO₂ at Lower Overpotential. *ACS Catal.* **2015**, *5*, 2521−2528.

(30) Vollmer, M. V.; Machan, C. W.; Clark, M. L.; Antholine, W. E.; Agarwal, J.; Schaefer, H. F.; Kubiak, C. P.; Walensky, J. R. Synthesis, Spectroscopy, and Electroche-mistry of (α-Diimine)M(CO)₃Br, M = Mn, Re, Complexes: Ligands Isoelectronic to Bipyridyl Show Differences in CO₂ Reduction. *Organometallics* **2015**, *34*, 3−12.

(31) Agarwal, J.; Shaw, T. W.; Schaefer, H. F., III; Bocarsly, A. B. Design of a Catalytic Active Site for Electrochemical CO₂ Reduction with Mn(I) Tri-carbonyl Species. *Inorg. Chem.* **2015**, *54*, 5285−5294.

(32) Stufkens, D. J.; van Outersterp, J. W. M.; Oskam, A.; Rossenaar, B. D.; Stor, G. J. The photochemical formation of organometallic radicals from α-diimine complexes having a metal-metal, metal-alkyl or metal-halide bond. *Coord. Chem. Rev.* **1994**, *132*, 147−154.

(33) Rossenaar, B. D.; Kleverlaan, C. J.; van der Ven, M. C. E.; Stufkens, D. J.; Oskam, A.; Fraanje, J.; Goubitz, K. Synthesis and spectroscopic properties of Re(R) (CO)₃(α-diimine) (R = alkyl; α-diimine = R′-pyCa, R′-DAB) complexes. Crystal structure of Re(Me) (CO)₃(ⁱPr-DAB). *J. Organomet. Chem.* **1995**, *493*, 153−162.

(34) Sieh, D.; Lacy, D. C.; Peters, J. C.; Kubiak, C. P. Reduction of CO₂ by Pyridine Monoimine Molybdenum Carbonyl Complexes: Cooperative Metal−Ligand Binding of CO₂. *Chem. - Eur. J.* **2015**, *21*, 8497−8503.

(35) Gonsalvi, L.; Gaunt, J. A.; Adams, H.; Castro, A.; Sunley, G. J.; Haynes, A. Quantifying Steric Effects of α-Diimine Ligands. Oxidative Addition of MeI to Rhodium(I) and Migratory Insertion in Rhodium(III) Complexes. *Organometallics* **2003**, *22*, 1047−1054.

(36) Machan, C. W.; Chabolla, S. A.; Kubiak, C. P. Reductive Disproportionation of Carbon Dioxide by an Alkyl-Functionalized Pyridine Monoimine Re(I) *fac*-Tricarbonyl Electrocatalyst. *Organometallics* **2015**, *34*, 4678−4683.

(37) Alvarez, C. M.; García-Rodríguez, R.; Miguel, D. Carbonyl complexes of manganese, rhenium and molybdenum with ethynylimi-nopyridine ligands. *J. Organomet. Chem.* **2007**, *692*, 5717−5726.

(38) Alvarez, C. M.; García-Rodríguez, R.; Miguel, D. Pyridine-2-carboxaldehyde as ligand: Synthesis and derivatization of carbonyl complexes. *Dalton Trans.* **2007**, 3546−3554.

(39) Bond, M.; Grabaric, B. S.; Grabaric, Z. Kinetic and Thermodynamic Study of Reactions of Some Substituted Manganese-(I) and Manganese(II) Tricarbonyl Complexes Using Spectrophoto-metric and Electrochemical Techniques. *Inorg. Chem.* **1978**, *17*, 1013−1018.

(40) Krause, L.; Herbst-Irmer, R.; Sheldrick, G. M.; Stalke, D. Comparison of silver and molybdenum microfocus X-ray sources for single-crystal structure determination. *J. Appl. Crystallogr.* **2015**, *48*, 3−10.

(41) Frisch, M. J.; Trucks, G. W.; Schlegel, H. B.; Scuseria, G. E.; Robb, M. A.; Cheeseman, J. R.; Scalmani, G.; Barone, V.; Mennucci, B.; Petersson, G. A.; Nakatsuji, H.; Caricato, M.; Li, X.; Hratchian, H. P.; Izmaylov, A. F.; Bloino, J.; Zheng, G.; Sonnenberg, J. L.; Hada, M.; Ehara, M.; Toyota, K.; Fukuda, R.; Hasegawa, J.; Ishida, M.; Nakajima, T.; Honda, Y.; Kitao, O.; Nakai, H.; Vreven, T.; Montgomery, J. A., Jr.; Peralta, J. E.; Ogliaro, F.; Bearpark, M.; Heyd, J. J.; Brothers, E.; Kudin, K. N.; Staroverov, V. N.; Kobayashi, R.; Normand, J.; Raghavachari, K.; Rendell, A.; Burant, J. C.; Iyengar, S. S.; Tomasi, J.; Cossi, M.; Rega, N.; Millam, J. M.; Klene, M.; Knox, J. E.; Cross, J. B.; Bakken, V.; Adamo, C.; Jaramillo, J.; Gomperts, R.; Stratmann, R. E.; Yazyev, O.; Austin, A. J.; Cammi, R.; Pomelli, C.; Ochterski, J. W.; Martin, R. L.; Morokuma, K.; Zakrzewski, V. G.; Voth, G. A.; Salvador, P.; Dannenberg, J. J.; Dapprich, S.; Daniels, A. D.; Farkas, Ö.; Foresman, J. B.; Ortiz, J. V.; Cioslowski, J.; Fox, D. J. *Gaussian 09*, Revision D.01; Gaussian, Inc., Wallingford, CT, 2013.

(42) Becke, A. D. Density-functional thermochemistry. III. The role of exact exchange. *J. Chem. Phys.* **1993**, *98*, 5648−5652.

(43) Lee, C.; Yang, W.; Parr, R. G. Development of the Colle-Salvetti correlation-energy formula into a functional of the electron density. *Phys. Rev. B: Condens. Matter Mater. Phys.* **1988**, *37*, 785−789.

(44) Nicklass, A.; Dolg, M.; Stoll, H.; Preuss, H. Ab initio energy-adjusted pseudopotentials for the noble gases Ne through Xe: Calculation of atomic dipole and quadrupole polarizabilities. *J. Chem. Phys.* **1995**, *102*, 8942−8952.

(45) Dunning, T. H., Jr.; Hay, P. J. In *Modern Theoretical Chemistry*; Schaefer, H. F., Ed.; Plenum Press: New York, 1977; Vol. 3.

(46) Krishnan, R.; Binkley, J. S.; Seeger, R.; Pople, J. A. Self-consistent molecular orbital methods. XX. A basis set for correlated wave functions. *J. Chem. Phys.* **1980**, *72*, 650−654.

(47) McLean, A. D.; Chandler, G. S. Contracted Gaussian basis sets for molecular calculations. I. Second row atoms, Z = 11−18. *J. Chem. Phys.* **1980**, *72*, 5639−5648.

(48) Mennucci, B.; Tomasi, J. Continuum solvation models: A new approach to the problem of solute's charge distribution and cavity boundaries. *J. Chem. Phys.* **1997**, *106*, 5151−5158.

(49) Cossi, M.; Barone, V.; Mennucci, B.; Tomasi, J. Ab initio study of ionic solutions by a polarizable continuum dielectric model. *Chem. Phys. Lett.* **1998**, *286*, 253−260.

(50) Bistoni, G.; Rampino, S.; Scafuri, N.; Ciancaleoni, G.; Zuccaccia, D.; Belpassi, L.; Tarantelli, F. How π back-donation quantitatively

controls the CO stretching response in classical and non-classical metal carbonyl complexes. *Chem. Sci.* **2016**, *7*, 1174−1184.